specific Cds1 paralog, Mek1, are required for this control. These regulatory genes, which are found to be required for normal levels of recombination, delay the onset into meiosis I in *meu13Δ* because they recognize the presence of unrepaired double-strand breaks (DSBs). Introducing excess DSBs in normal cells by γ-ray irradiation similarly delayed the onset of meiosis. Furthermore, *radΔ meu13Δ*, *cds1Δ meu13Δ* and *mek1Δ meu13Δ* double mutants exhibited decreased recombination frequencies and reduced spore viability, indicating that *rad⁺*, *cds1⁺* and *mek1⁺* act to delay the cell's progression into meiosis I until the DSBs are repaired. Thus, we propose that a meiotic recombination checkpoint exists in *S.pombe* to ensure the production of viable spores and recombination at the proper frequencies.

Results

Meiotic progression is delayed in the meu13Δ and dmc1Δ mutants

In budding yeast, nematodes (*Caenorhabditis elegans*), flies (*Drosophila melanogaster*) and mice, some of the mutant cells that are defective in recombination and/or synapsis will arrest at the pachytene stage (Roeder and Bailis, 2000). In fission yeast, however, so far it has not been determined whether a failure to complete meiotic recombination will affect the meiotic progression. To investigate whether meiotic recombination-deficient mutants show any defect in meiotic progression, we checked the meiotic progression of two meiotic recombination-deficient mutants, *meu13Δ* and *dmc1Δ*. *meu13⁺* and *dmc1⁺* have both been identified as meiosis-specific genes (Watanabe *et al.*, 2001). *meu13⁺* is a budding yeast *HOP2* homolog and is required for proper homologous pairing and recombination (Nabeshima *et al.*, 2001). *dmc1⁺*, a meiotic RecA homolog conserved among a variety of organisms, also participates in fission yeast meiotic recombination (Fukushima *et al.*, 2000). To synchronize meiosis effectively, we used the *pat1-114* temperature-sensitive strain, which enters meiosis in a highly synchronous manner when it is shifted to its restrictive temperature (Iino and Yamamoto, 1985). Homozygous diploid *pat1*, *pat1 meu13Δ* and *pat1 dmc1Δ* cells were arrested at the G₁ stage by nitrogen starvation and then shifted to the restrictive temperature to induce synchronous meiosis (Figure 1A). Meiotic recombination occurs at the horsetail stage (orange line in Figure 1A), where the nucleus repeatedly moves backwards and forwards several times. The time at which the horsetail stage developed was similar for all three strains (~2 h after temperature shift, peaking at ~3 h). Thus, neither *meu13Δ* nor *dmc1Δ* appear to affect the entry into meiotic prophase in *pat1* cells. However, in the *pat1 meu13Δ* and *pat1 dmc1Δ* double mutants, meiosis I peaked 6 h after the temperature shift, 30 min later than for *pat1*. Cumulative curves (Hunter and Kleckner, 2001) clearly showed that in *pat1 meu13Δ* and *pat1 dmc1Δ* mutants, entry into the horsetail stage was similar to that in *pat1*, but both exit from the horsetail stage and entry into meiotic division were delayed (Figure 1B). This delay in meiosis I initiation was observed in more than four independent experiments performed identically.

The delay in meiotic progression of meu13Δ but not dmc1Δ is dependent on Rec12/Spo11

The observations above suggest that the deficiency in meiotic homologous recombination in the *meu13Δ* and *dmc1Δ* mutants is responsible for the delay in meiotic progression. If so, this delay should be dependent on the initiation of recombination. It is known that the formation of DSBs is required for the initiation of meiotic recombination and that *rec12⁺* of *S.pombe*, which encodes a protein homologous to Spo11 of *S.cerevisiae*, is essential for the generation of DSBs (Cervantes *et al.*, 2000). Thus, we examined whether the delay in the meiotic progression of the *meu13Δ* and *dmc1Δ* mutants is dependent on *rec12⁺*. The average percentages of cells in meiosis I at 5 and 6 h are shown in Figure 1C. Deletion of *rec12⁺* eliminated the delay that was observed in *pat1 meu13Δ* cells and allowed these cells to enter into meiosis I with the same kinetics as seen in *pat1*. Thus, the delay in meiotic progression observed in *meu13Δ* is dependent on *rec12⁺*, namely on the initiation of recombination. This suggests that recombination intermediates in *meu13Δ* trigger a meiotic delay.

Interestingly, the deletion of *rec12⁺* did not eliminate the *dmc1Δ* delay but caused more delay than *pat1 dmc1Δ* (Figure 1C), suggesting that the meiotic delay in these cells is independent of the initiation of recombination and that it may be triggered by a signal other than recombination intermediates (see Discussion).

rad17⁺, rad3⁺, rad1⁺ and rad9⁺ genes participate in delaying meiotic progression in meu13Δ but not in dmc1Δ

Checkpoint *rad⁺* genes (*rad1⁺*, *rad3⁺*, *rad9⁺*, *rad17⁺*, *rad26⁺* and *hus1⁺*), *crb2⁺/rhp9⁺*, *cds1⁺* and *chk1⁺* act in the DNA damage and/or DNA replication checkpoint controls (Caspari and Carr, 1999). Unrepaired DNA or a block in replication are sensed by these genes, which then act to stop or delay the cell cycle progression by transmitting the checkpoint signals to Cdc2 kinase, a major regulator of the G₂/M transition. In *S.cerevisiae*, it has been reported that some of the homologs of fission yeast checkpoint genes also control meiotic progression (Lydall *et al.*, 1996). Thus, we investigated if these fission yeast checkpoint genes could be participating in the delay of meiotic progression observed in the *meu13⁺* and *dmc1⁺* mutants. As shown in Figure 1C, the deletion of *rad17⁺* abolished the delay observed in *pat1 meu13Δ* cells and allowed these cells to enter meiosis I with a timing similar to that observed in *pat1*. Deletion of *rad1⁺*, *rad3⁺* and *rad9⁺* also eliminated the delay of *pat1 meu13Δ* (data not shown). Thus, *rad17⁺*, *rad3⁺*, *rad1⁺* and *rad9⁺* genes participate in the delay of meiotic progression in *meu13Δ*. In the damage checkpoint, checkpoint *rad⁺* genes are thought to monitor DNA damage such as DSBs and respond to this damage by delaying cell cycle progression (Caspari and Carr, 1999). Thus, these data, together with the observation in the previous section that lack of the ability to produce DSBs normalizes *meu13Δ* meiosis, suggest that *meu13Δ* cells may accumulate DSBs that are monitored by these checkpoint genes.

Saccharomyces cerevisiae dmc1Δ cells are known to accumulate DSBs during recombination intermediate stages (Bishop *et al.*, 1992). Given that this mutant, like the *dmc1Δ* mutant of *S.pombe* (Fukushima *et al.*, 2000),

also exhibits a decreased frequency of meiotic recombination, we expected that *S.pombe dmc1Δ* cells would also accumulate DSBs and that these might trigger the meiotic delay in *dmc1Δ* cells. However, the deletion of *rad17+*, *rad1+*, *rad3+* and *rad9+* did not eliminate the delay in meiotic progression of the *pat1 dmc1Δ* mutant but caused a much greater delay than *pat1 dmc1Δ* (Figure 1C and data not shown). This again indicates that the regulation of the meiotic delay observed in *dmc1Δ* is different from that in *meu13Δ* cells.

rad3+ and *rad17+* increase the viability of the meiotic product and the recombination frequency in recombination mutants

Because checkpoint *rad+* genes participate in controlling meiotic progression in *meu13Δ* and *dmc1Δ*, checkpoint *rad+* deletion in *meu13Δ* and *dmc1Δ* would affect their production of viable meiotic products. As shown in Figure 2A, the spore viability of *rad3Δ* and *rad17Δ* was similar to that of wild-type cells, whereas *rad3Δ meu13Δ*, *rad17Δ meu13Δ* and *rad17Δ dmc1Δ* double mutants showed a reduced spore viability when compared with their corresponding single mutant. The number of spores with more than four 4′,6-diamidino-2-phenylindole (DAPI)-stained masses was greater in the *rad17Δ meu13Δ* and *rad17Δ dmc1Δ* double mutants than in the single mutants (Figure 2C), suggesting more frequent fragmentation in double mutants. Thus, spore viabilities were reduced by the disruption of *rad3+* and *rad17+* in meiotic recombination mutants, although the mechanism operating in *meu13Δ* is different from that in *dmc1Δ*.

Next we examined whether the disruption of *rad3+* and *rad17+* decreases the frequency of recombination in the *meu13Δ* and *dmc1Δ* mutants by measuring the frequency of allelic gene conversion between two different mutant alleles of *ade6*, namely *ade6-M26* and *ade6-469*, in these double mutants (Figure 2B). We found that the *rad3Δ* and *rad17Δ* single mutants already had a reduced recombination frequency, as shown by a decrease in the percentage of Ade+ recombinant spores relative to the wild-type strain. Thus, the *rad3+* and *rad17+* genes are required to maintain a normal level of meiotic recombination even in normal cells. The double mutants also exhibited a decrease in recombination. For example, recombination in *rad3Δ meu13Δ* and *rad17Δ meu13Δ* was decreased to 44 and 34% of that of *meu13Δ*. The *rad17Δ dmc1Δ* mutant also showed a reduced recombination frequency as compared with the single mutants. Thus, Rad3 and Rad17 are needed in the *meu13Δ* and *dmc1Δ* mutants to allow sufficient levels of recombination to occur so that viable spores can be produced.

cds1+ and *mek1+* participate in maintaining spore viability and recombination frequency and delaying meiotic progression in the *meu13Δ* mutant

The *MEK1* gene of *S.cerevisiae* encodes a meiosis-specific protein kinase that participates in the pachytene checkpoint (Rockmill and Roeder, 1991). We isolated a fission yeast homolog (*mek1+*) of *MEK1* by computer-assisted homologous searching in GenBank. The *mek1+* gene was then isolated by PCR using appropriate primers and the

genomic DNA of *S.pombe* as a substrate (T.Tougan, M.Shimada and H.Nojima, unpublished data). We found that the Ade+ frequencies of *cds1Δ* and *mek1Δ* were only 48 and 33% that of the wild-type strain, respectively, suggesting that Cds1 and the fission yeast Mek1 homolog are also required to maintain normal levels of meiotic recombination in wild-type cells (Figure 2B). However, the viabilities of *cds1Δ* and *mek1Δ* spores were 91 and 94% that of the wild-type strain, respectively. Thus, spore viability was not affected by these mutations as by the *rad3Δ* and *rad17Δ* mutations (Figure 2A). Both *cds1Δ meu13Δ* and *mek1Δ meu13Δ* double mutants, however, exhibited reduced levels of spore viability and meiotic recombination. Thus, when there is already a partial defect in meiotic recombination, the *cds1+* and *mek1+* genes are also required to generate enough meiotic recombination to ensure spore viability (Figure 2A and B). Furthermore, deletion of *cds1+* and *mek1+* genes also eliminated the delay of *pat1 meu13Δ* cells, indicating that both *cds1+* and *mek1+* genes have a function in controlling meiotic progression in *pat1 meu13Δ* cells like checkpoint *rad+* genes.

Meiotic DSB repair is delayed in *meu13Δ*

Considering that the meiotic delay of *meu13Δ* is dependent on *rec12+* as well as on checkpoint *rad+* genes, which monitor such damage, we surmised that the meiotic delay is triggered by the accumulation of recombination intermediates such as DSBs. To test this possibility directly, we examined the formation of DSBs during meiosis in the *meu13Δ* strain by pulsed-field gel electrophoresis (PFGE). In fission yeast, meiotic DSBs can be detected as smeared bands by PFGE because they produce broken chromosomes with variable length (Cervantes *et al.*, 2000). In the *pat1 meu13Δ* and *pat1 dmc1Δ* double mutants, as well as in the *pat1* single mutant strain, smeared bands appeared 3 h after the temperature shift (Figure 3). This result is consistent with that shown in Figure 1A, which suggests that the double mutant cells enter the meiotic prophase at approximately the same time after shifting the temperature as *pat1* cells. Smeared bands were no longer observed in *pat1* cells 4.5 h after the temperature shift but they continued to be observed in *pat1 meu13Δ* cells. Thus, meiotic DSB repair is delayed in *pat1 meu13Δ*.

Unexpectedly, the smeared bands in *pat1 dmc1Δ* cells were diminished 4.5 h after the temperature shift, as in the *pat1* strain (Figure 3). This suggests that defects other than a delay in DSB repair may be triggering the delay in meiosis in *dmc1Δ*, which is consistent with the fact that the checkpoint *rad+* genes also do not appear to be involved.

pat1 rad17Δ meu13Δ cells had smeared bands at the time point when they would be entering meiosis I (Figures 3 and 1), suggesting that *pat1 rad17Δ meu13Δ* cells probably enter meiosis I without completing DSB repair, which would cause chromosome fragmentation. In line with this is that this strain produced abnormal spores with an irregular number of DAPI-stained bodies, as shown in Figure 2C. To assess whether the smeared bands observed here are specific to meiotic recombination, we examined the effect of disrupting *rec12+* on the presence of smeared bands, as *rec12+* is responsible for introducing

2809

DSBs during meiosis. The *rec12Δ meu13Δ* double mutant never shows smeared bands at any time (Figure 3). These results strongly support the idea that the broken chromosomes, which were observed in *rad17Δ meu13Δ* meiosis I, were caused by meiotic DSBs, and that *rad17⁺* acts to delay *meu13Δ* from entering meiosis I to allow the DSBs to be repaired.

γ-ray irradiation of wild-type cells during the horsetail period delays their entry into meiosis I in a *rad17⁺*-dependent manner

If the delay in entering meiosis I in *meu13Δ* cells is caused by the persistent presence of DSBs, one would expect that an increased number of DSBs formed during the meiotic prophase would cause even wild-type cells to experience a
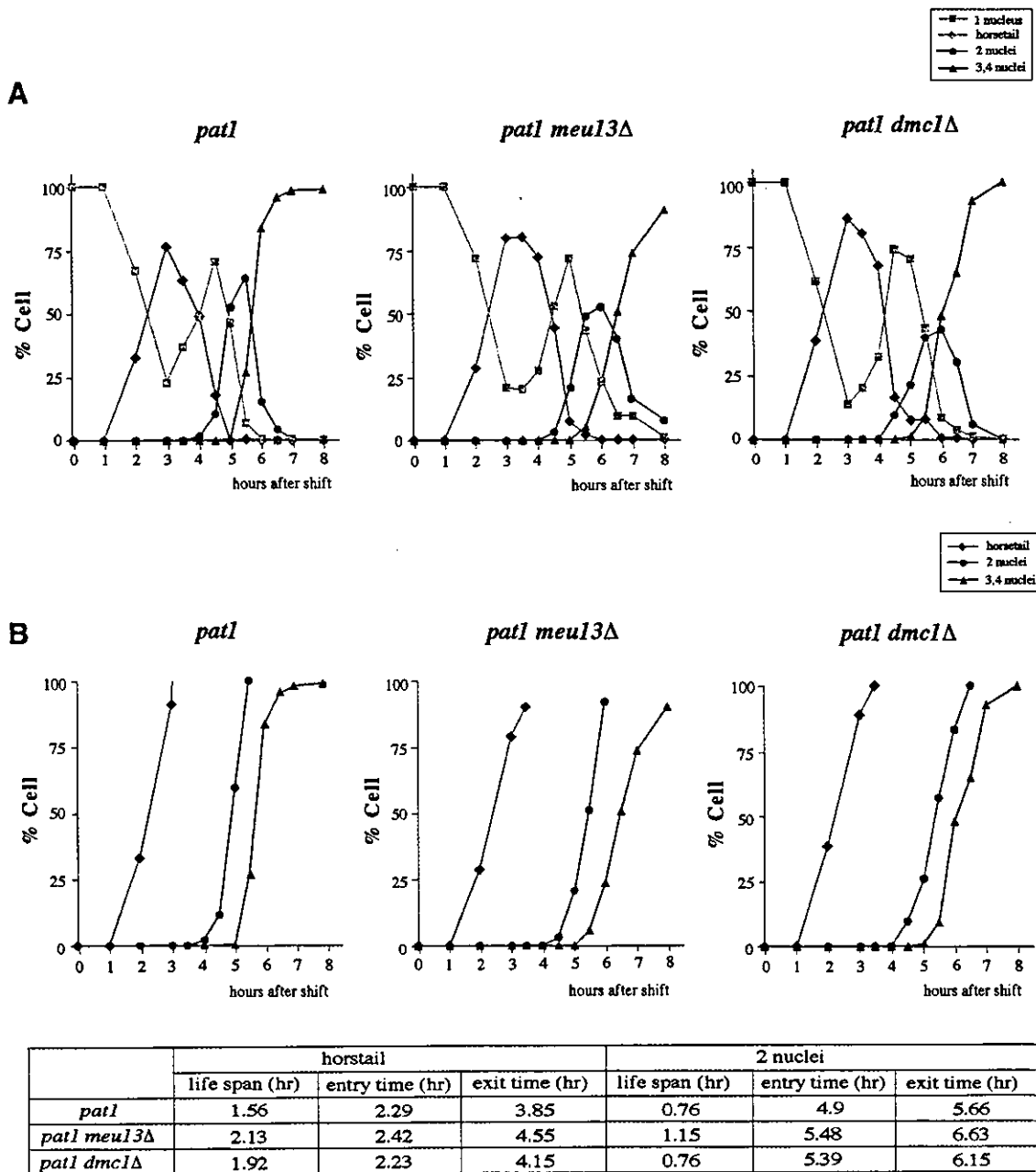

Fig. 1. Meiotic recombination-deficient mutants, *meu13Δ* and *dmc1Δ*, are delayed in entering meiosis I. (A) Homozygous diploid *pat1* cells were cultured to mid log phase, transferred to EMM-N medium for 16 h at 25°C and then shifted to 34°C to inactivate Pat1 and synchronize meiosis. Progression of meiosis was monitored by DAPI staining of samples that were collected every 30 min or 1 h after temperature shift. At least 150 cells were scored by fluorescence microscopy for each time point. (B) Cumulative curves and the time indicating the life span, entry into and exit from each DNA stage of *pat1*, *pat1 meu13Δ* and *pat1 dmc1Δ*. Cumulative curves are expressed as a percentage of maximum values against time after temperature shift (Hunter and Kleckner, 2001). (C) Meiotic delay of *meu13Δ* is dependent on the *rec12⁺* gene and checkpoint *rad⁺* genes but this is not the case for *dmc1Δ*. Cells were induced to enter meiosis and the progression of meiosis was monitored by DAPI staining. Shown are the average ratios of cells in meiosis I at 5 and 6 h in three or four independent experiments. (D) γ-ray-irradiated cells are delayed in entering meiosis I and this delay is also dependent on *rad17⁺*. Cells were induced to enter meiosis and irradiated with γ-rays 3 h after temperature shift, when the cells were in the horsetail period. Shown are the average ratios of cells in meiosis I at 5.5 h in three independent experiments. Strains: *pat1* (JZ670), *pat1 meu13Δ* (KN8), *pat1 dmc1Δ* (MS276-1), *pat1 rec12Δ* (MS123-5), *pat1 rec12Δ meu13Δ* (MS110-2), *pat1 rec12Δ dmc1Δ* (MS189-1), *pat1 rad17Δ* (MS101-4), *pat1 rad17Δ meu13Δ* (MS107-1), *pat1 rad17Δ dmc1Δ* (MS190-7), *pat1 cds1Δ meu13Δ* (MS231-1) and *pat1 mek1Δ meu13Δ* (MS217-1).

2810

delay in entering meiosis I. To examine this possibility, we irradiated meiotic *pat1* cells during the horsetail period with γ-rays (3 h after temperature shift) and determined when these cells entered meiosis I. As shown in Figure 1D, the onset of meiosis I was delayed in irradiated *pat1* cells relative to non-irradiated cells. However, when *rad17*⁺ was deleted from *pat1* cells, γ-ray irradiation no longer affected the timing with which meiosis I was initiated.
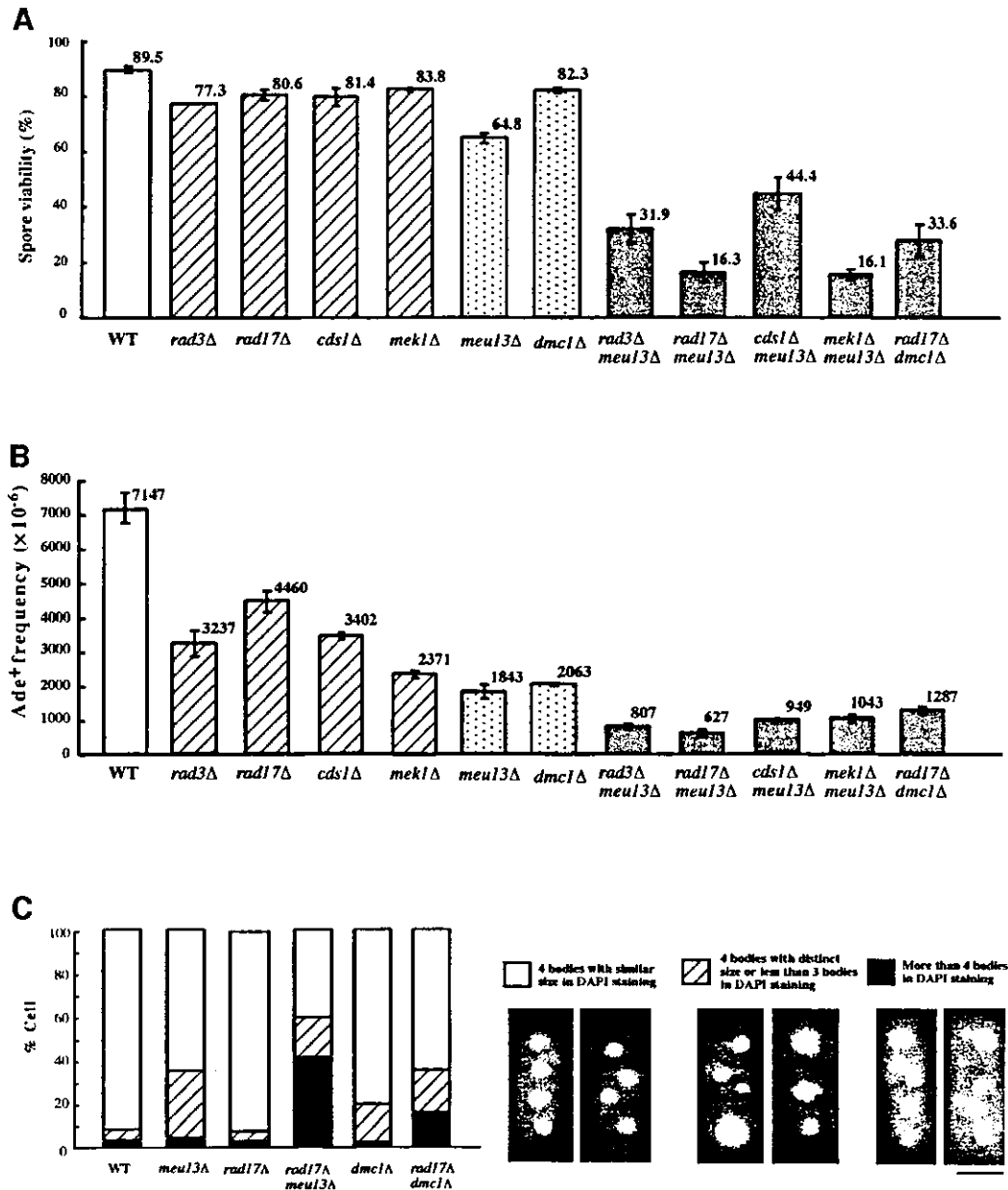
A

B

C
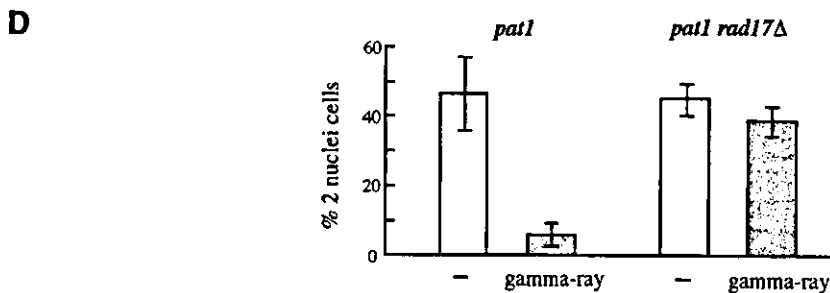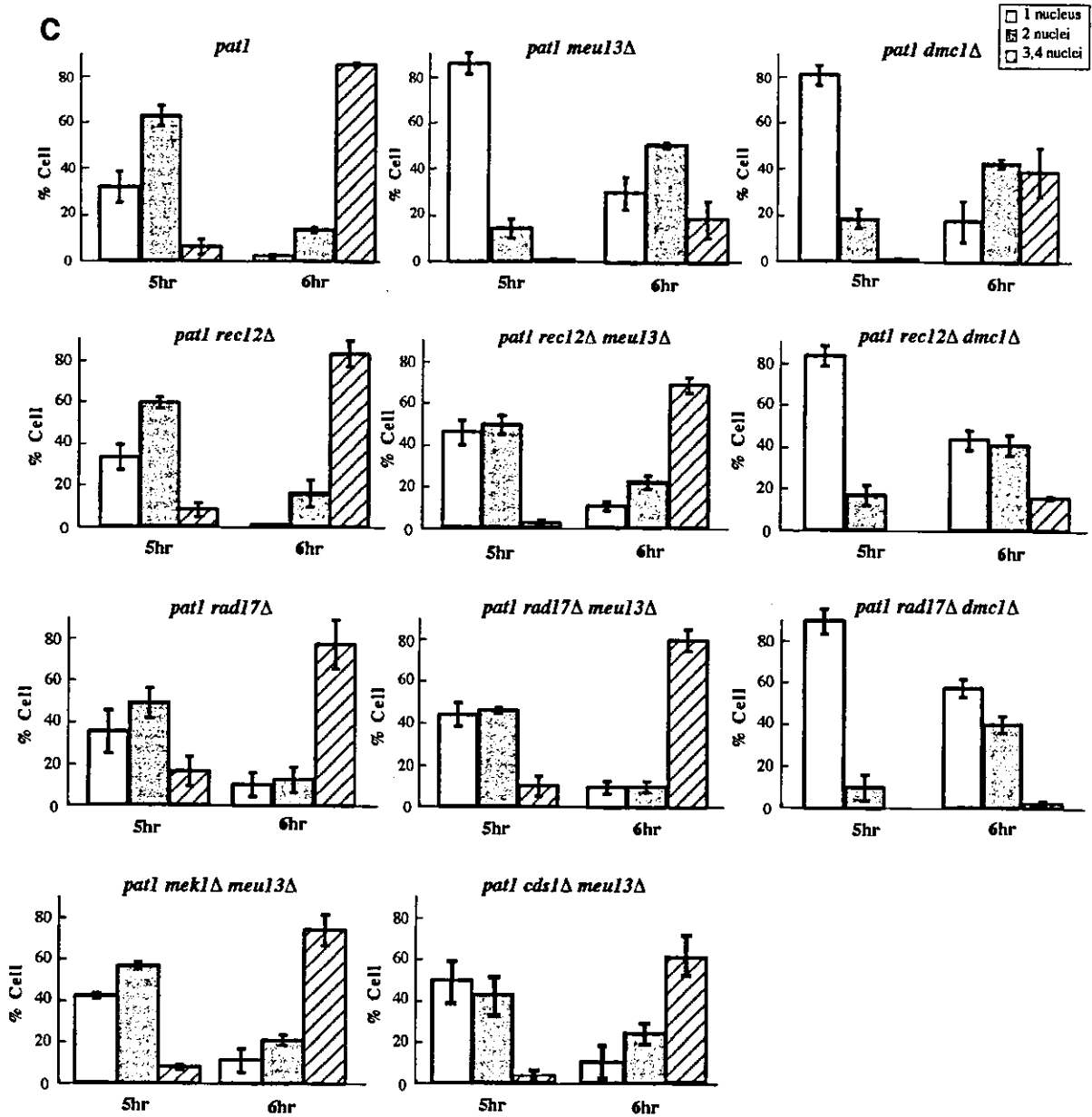
Fig. 2. Spore viability and gene conversion frequencies of meiosis-defective mutants. The spore viabilities (A) and allelic gene conversion frequencies (B) between *ade6-469* and *ade6-M26* of double mutants (*rad3Δ meu13Δ, rad17Δ meu13Δ, cds1Δ meu13Δ, mek1Δ meu13Δ* and *rad17Δ dmc1Δ*) and single mutants were measured. The various strains were generated by crossing wild-type (MS111-W1 × MS105-1B), *rad3Δ* (MS126-4 × MS162-1), *rad17Δ* (MS111-1 × MS105-22D), *cds1Δ* (MS233-4 × MS245-3), *mek1Δ* (MS203-2 × MS202-11), *meu13Δ* (MS111-m13 × MS105-22C), *dmc1Δ* (MS133-1 × MS114-3), *rad3Δ meu13Δ* (MS128-15 × MS163-10), *rad17Δ meu13Δ* (MS111-6 × MS105-25C), *cds1Δ meu13Δ* (MS233-3 × MS245-7), *mek1Δ meu13Δ* (MS203-2 × MS202-10) and *rad17Δ dmc1Δ* (MS133-1 × MS114-3). All data presented above are the average of three independent experiments with standard errors. (C) The phenotype of wild-type, *meu13Δ, rad17Δ, rad17Δ meu13Δ, dmc1Δ* and *rad17Δ dmc1Δ* cells. Typical microscopic images of the asci stained by DAPI are shown in the right panels. The scale bar represents 5 μm.

Thus, DSBs appear to be monitored by a checkpoint pathway involving *rad17+*, and their presence delays the cell's entry into meiosis I.

Phosphorylation of Tyr15 in Cdc2 is maintained for a longer period in *pat1 meu13Δ* than in *pat1*

Phosphorylation of Tyr15 in Cdc2 plays a key role in blocking the onset of mitosis when DNA replication is inhibited or DNA is damaged (Rhind *et al.*, 1997; Rhind and Russell, 1998). To investigate whether this phosphorylation participates in delaying meiosis in *meu13Δ* cells, we monitored Cdc2 Tyr15 phosphorylation in *pat1* and *pat1 meu13Δ* cells during meiosis and sporulation (Figure 4). The level of the phosphorylated form of Cdc2 increased during the pre-meiotic S phase and decreased during meiotic division in *pat1* cells. In *pat1 meu13Δ* cells, however, Cdc2 was phosphorylated for 1 h longer than in *pat1* cells, consistent with the length of the delay in
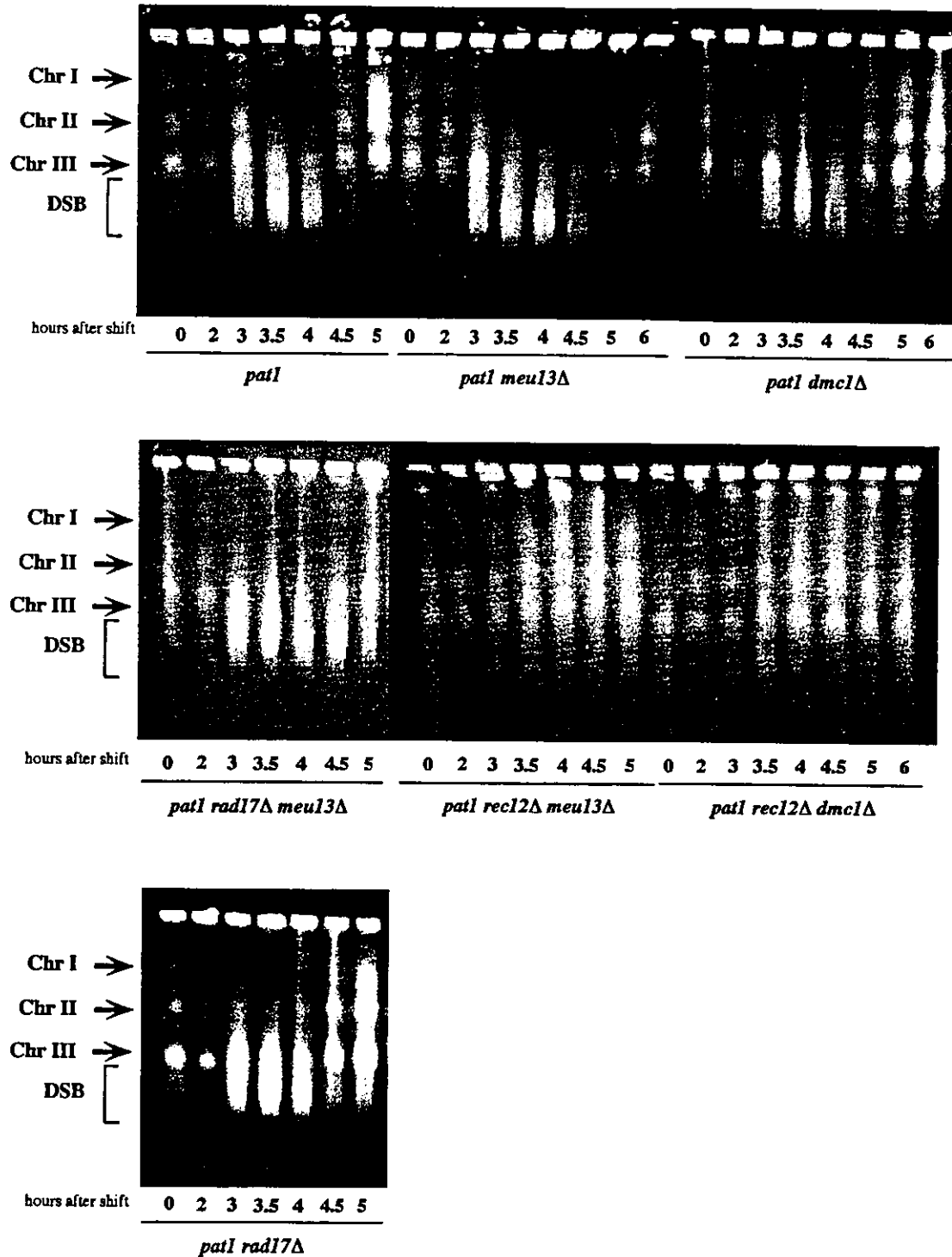
2812

Fig. 3. DSB repair is retarded in *meu13Δ*. Cells were induced to enter meiosis as shown in Figure 2. Samples were taken after the temperature shift at the indicated time points, analyzed by PFGE and stained with ethidium bromide to detect DNA. Chr I, Chr II and Chr III indicate the position of chromosomes 1, 2 and 3, respectively. The smear bands represent the DSBs that appear during meiosis.

meiosis I onset in *pat1 meu13Δ* cells. Furthermore, we found that this extended period of phosphorylation was not present in *pat1 rad17Δ meu13Δ* and *pat1 rec12Δ meu13Δ* cells, which do not experience a delay in meiosis, as shown in Figure 1C. Thus, the regulatory pathway delaying the onset of meiosis I in *meu13Δ* employs the phosphorylation of Tyr15 in Cdc2.

Three protein kinases, Cds1, Chk1 and Mek1, are expressed and phosphorylated during meiosis

Cds1 and Chk1 play important roles in checkpoint controls and are phosphorylated when the checkpoints are activated. Thus, we examined the expression of Cds1, Chk1 and Mek1 (the meiotic paralog of Cds1) during meiosis and sporulation in *pat1* and *pat1 meu13Δ* cells (Figure 5). In
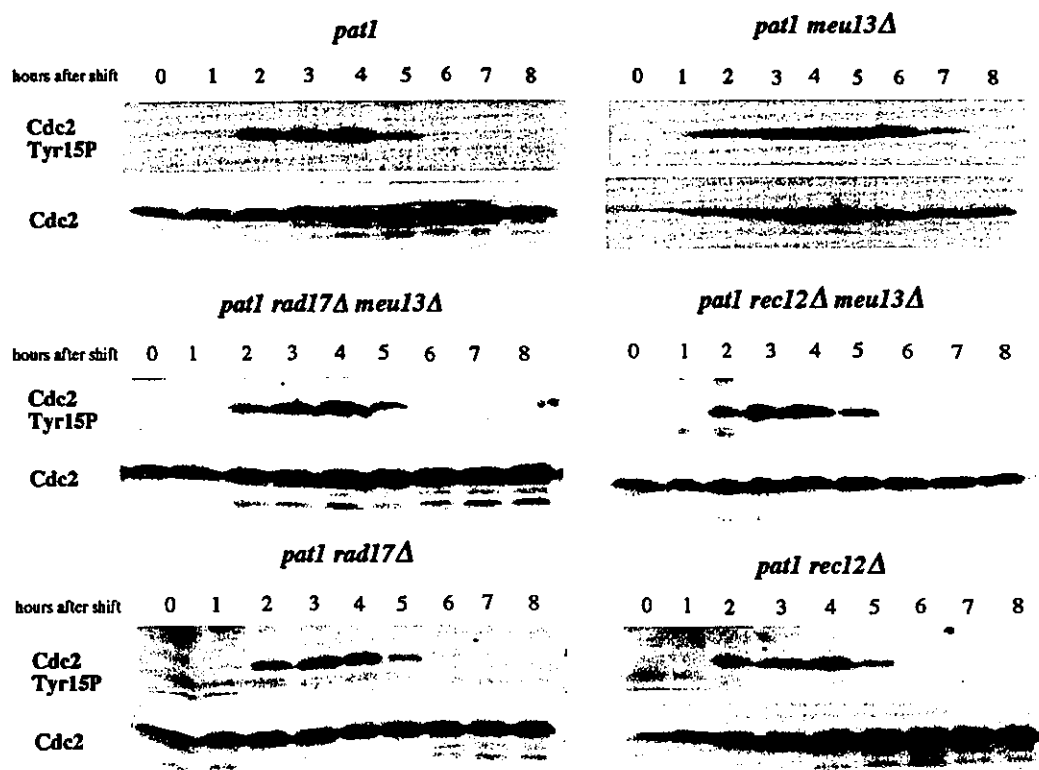
2813

Fig. 4. Phosphorylation of the Tyr15 in Cdc2 is extended in *pat1 meu13Δ. pat1* (JZ670), *pat1 meu13Δ* (KN8), *pat1 rec12Δ meu13Δ* (MS110-2), *pat1 rad17Δ meu13Δ* (MS107-1), *pat1 rec12Δ* (MS123-5) and *pat1 rad17Δ* (MS101-4) cells were induced to enter meiosis as shown in Figure 1. Samples were taken after the temperature shift at the indicated time points and western blot analysis was performed to detect the amount of Cdc2 and phosphorylated Cdc2.

both *pat1* and *pat1 meu13Δ* cells, Cds1 was phosphorylated from 2 h after the temperature shift, which continued to the end of sporulation. In both cell types, Chk1 was not phosphorylated during early meiosis but was phosphorylated slightly in the later stage. However, Mek1 was expressed only during pre-meiotic replication and meiotic recombination and showed a mobility shift during these periods, suggesting that phosphorylation occurred. Furthermore, the extent of Mek1 mobility shift in *pat1 meu13Δ* is greater than that in *pat1*, whereas the expression patterns of Cds1 and Chk1 are similar in these cells at the time point just before the onset of meiosis I (Figure 5; 4 h). These results suggest that Cds1, Chk1 and Mek1 have different functions during meiosis.

Discussion

The meiotic recombination checkpoint exists in fission yeast

In this study, we found that *meu13Δ* cells harboring a defect in meiotic recombination had a delay in the entry into meiosis I. The delay was dependent on *rec12+/SPO11*, which is required for initiation of meiotic recombination, *rad17+*, *rad1+*, *rad3+* and *rad9+*, which are required for damage and replication checkpoints in mitosis, *cds1+*, and *mek1+*, a meiosis-specific *cds1+* paralog. Furthermore, we found that there is a delay in meiotic DSB repair in *meu13Δ*. From these results, we surmised that a delay, elicited by DNA damage and replication checkpoint genes, was required in *meu13Δ* cells to repair meiotic DSBs

before their entry into meiosis I. Consistent with this hypothesis, deletion of *rad17+* allowed *meu13Δ* cells to progress into meiosis I without completing DSB repair. These results strongly suggest that, when meiotic DSB repair is delayed in *S.pombe*, DSBs are detected by DNA damage and replication checkpoint genes, which retards meiotic progression. To test this hypothesis directly, we artificially introduced an unusually large amount of DSBs into meiotic cells. This triggered a delay in meiotic progression, which was dependent on *rad17+* (Figure 1D). Taken together, we propose that a meiotic recombination checkpoint exists in *S.pombe* to monitor meiotic DSB repair and regulate entry into meiosis I (Figure 6). This regulation seems to be responsible for the maintenance of the optimal level of spore viability and meiotic recombination frequency in cells that experience a delay in DSB repair (Figure 2).

In budding yeast, *S.cerevisiae*, it has been reported that the pachytene checkpoint operates to arrest cells at the pachytene stage in response to a defect in recombination and/or synapsis. It has not been shown clearly, however, whether meiotic delay is triggered by a defect in DSB repair or synaptonemal complex formation, or by defects in both of them together (Roeder and Bailis, 2000). Of note is that in striking contrast to *S.cerevisiae*, *S.pombe* does not form any SC (Bahler *et al.*, 1993). Considering that many genes required for the meiotic recombination checkpoint in *S.pombe* have homologs that are required for the pachytene checkpoint in *S.cerevisiae*, and the strong analogy between the observations in these two
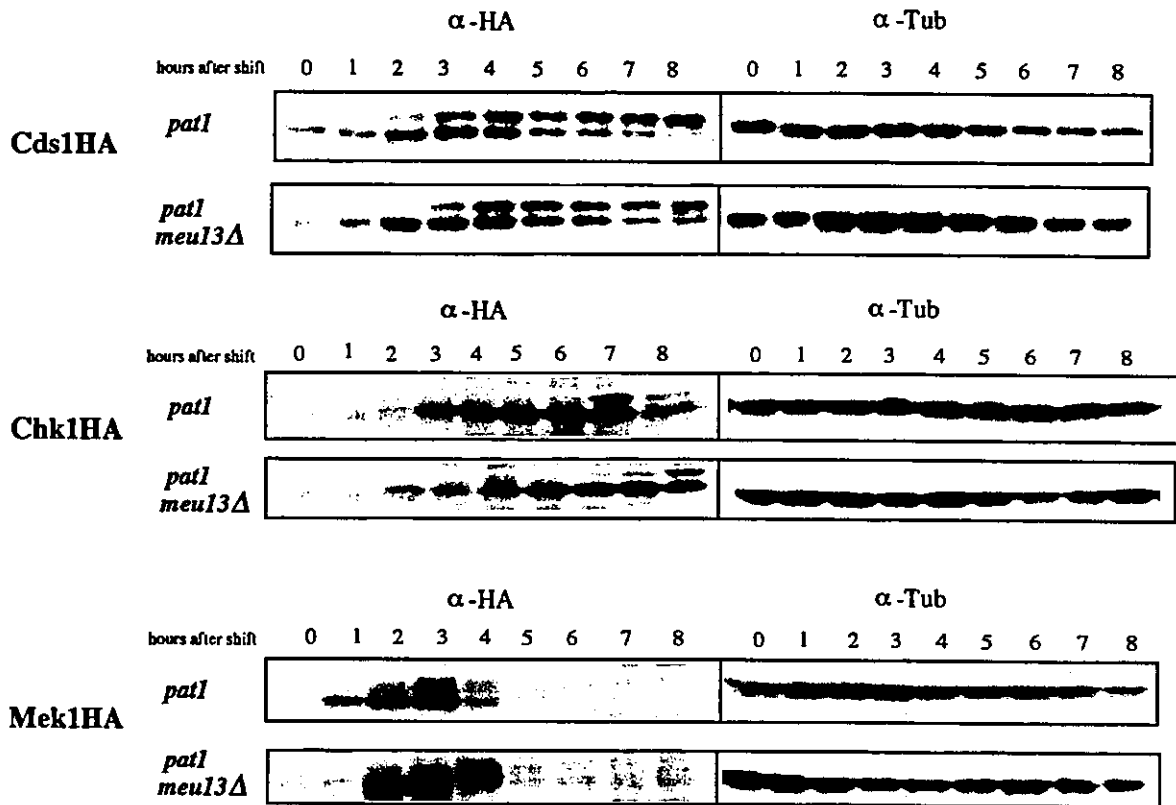
2814

Fig. 5. Three protein kinases, Cds1, Chk1 and Mek1, are expressed and phosphorylated during meiosis and sporulation in fission yeast. *pat1* Cds1HA (MS197-6), *pat1 meu13Δ* Cds1HA (MS198-1), *pat1* Chk1HA (MS108-1), *pat1 meu13Δ* Chk1HA (MS196-2), *pat1* Mek1HA (MS199-4) and *pat1 meu13Δ* Mek1HA (MS200-5) cells were induced to enter meiosis as shown in Figure 1. Samples were taken after the temperature shift at the indicated time points and proteins were prepared and detected with anti-HA and anti α-tubulin antibodies.

yeasts, our results strongly suggest that the checkpoint actually monitors defects in meiotic recombination.

The role of the checkpoint *rad⁺* genes, *cds1⁺* and *mek1⁺* in meiotic recombination

We report here that *S.pombe rad17⁺*, *rad3⁺*, *cds1⁺* and *mek1⁺* genes are required for maintaining a normal level of meiotic recombination, although they are not required for the maintenance of viable spores (Figure 2 and Murakami and Nurse, 1999). This is consistent with the notion that many DNA damage checkpoint genes may play a direct role in meiotic recombination in other species. In *S.cerevisiae*, genes homologous to *S.pombe rad17⁺*, *rad3⁺* and *mek1⁺* are required for meiotic recombination (Kato and Ogawa, 1994; Lydall *et al.*, 1996; Xu *et al.*, 1997). Mammalian Rad1, ATR, ATM and Chk1 (*S.pombe rad1⁺*, *rad3⁺*, *tel1⁺* and *chk1⁺* homologs, respectively) have been found to localize to synapsed and/or unsynapsed meiotic chromosomes (Roeder and Bailis, 2000) and are suggested to play a direct role in meiotic recombination.

Schizosaccharomyces pombe Mek1, which is expressed only during meiosis, is required for efficient meiotic recombination. Mek1 is also required for the meiotic recombination checkpoint (Figure 1C). In *S.cerevisiae*, Mek1 is considered to be the meiotic counterpart of Rad53 (*S.pombe* Cds1 homolog). However, the meiotic function of Rad53 is not fully understood. *Schizosaccharomyces pombe* Cds1 is required for a normal level of meiotic

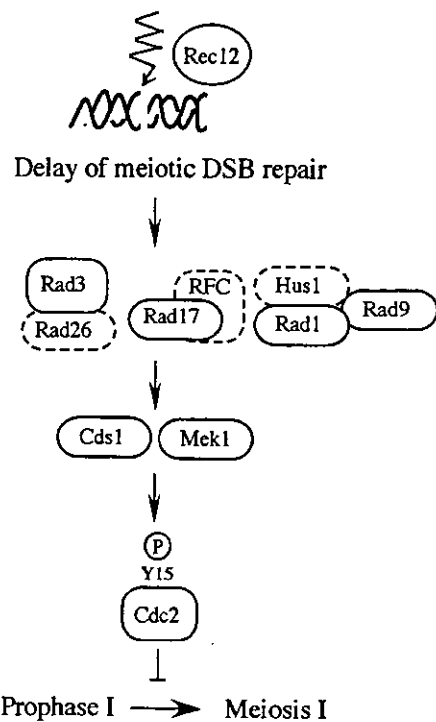

Delay of meiotic DSB repair

Prophase I ⟶ Meiosis I

Fig. 6. A model of the meiotic recombination checkpoint in fission yeast. When repair of meiotic DSBs is retarded, checkpoint *rad⁺*, *cds1⁺* and *mek1⁺* genes delay cells to enter into meiosis I through phosphorylation of Cdc2 Tyr15 to provide enough time to repair DSBs.

2815

recombination. Cds1 is also required for maintaining spore viability and recombination efficiency in *meu13Δ* (Figure 2). Therefore, we conclude that both Mek1 and Cds1 are required for the meiotic recombination checkpoint in *S.pombe*.

Phosphorylation of Cds1 is observed from the initiation of pre-meiotic replication (2 h after temperature shift) through to the end of sporulation. Chk1 expression strongly increases after the first meiotic division, but Chk1 only becomes phosphorylated at the sporulation stage (Figure 5). Mek1 expression begins at the start of pre-meiotic replication and continues until about the time of meiosis I. Mek1 displays a mobility shift during these periods, which is probably due to its phosphorylation, as was shown previously in *S.cerevisiae* (Rockmill and Roeder, 1991). Thus, the meiotic regulation of each of these three protein kinases, Cds1, Chk1 and Mek1, is possibly different in terms of expression and phosphorylation, suggesting that each has a distinct role to play in meiosis. From these results, we speculate that Rad17, Rad3, Cds1 and Mek1 may be involved in some part of the DNA recombination process as well as in the meiotic recombination monitoring system.

In addition to the homology to the above-mentioned genes, the targets of these checkpoints seem to be the same. In *S.cerevisiae*, entry into meiosis I is inhibited by maintaining the Tyr19-phosphorylated state of Cdc28 (*S.pombe* Cdc2 homolog) in response to activation of the pachytene checkpoint because the Tyr19-non-phosphorylated form mutants cannot arrest properly in such a situation (Leu and Roeder, 1999; Tung *et al.*, 2000). We confirmed that similar regulation of Cdc2 operates in *S.pombe*; the timing of Tyr15 phosphorylation of Cdc2 is retarded when entry into meiosis I is delayed in the *meu13Δ* mutant (Figure 4).

What is the defect that triggers a meiotic delay in *dmc1Δ* cells?

We showed here that *S.pombe dmc1Δ* cells display the following unexpected phenotypes as compared with those of *S.cerevisiae*. First, *dmc1Δ* cells show a delay in meiotic progression but do not arrest at prophase as seen in *S.cerevisiae* (Figure 1). Second, they do not exhibit accumulation of DSBs (Figure 3). Third, the level of reduction in recombination or spore viability is much less than those of the *dmc1* mutant of *S.cerevisiae* (Figure 2).

Meiotic delay in *dmc1Δ* cells is not alleviated by elimination either of DSBs by deletion of *rec12⁺* or of the checkpoint genes involved in the delay in *meu13Δ* cells (Figure 1C). These results imply that Dmc1 plays a role in *S.pombe* meiosis that is independent of DSB formation. They also mean that the absence of this DSB-independent role triggers a delay in meiotic progression which is distinct from that mediated by the functions of the DNA damage checkpoint.

We surmise the following possibilities to explain why *dmc1Δ* shows meiotic delay. First, *S.pombe dmc1⁺* may play a role in recombination independent of DSB formation, which might be single-strand break-induced recombination. Second, the defect of *dmc1⁺* function may alter chromatin structure to inhibit proper division of the nucleus, which requires time to be repaired. Third, like *S.cerevisiae SPO11* and *REC8*, mutations of which affect

the duration of pre-meiotic replication (Cha *et al.*, 2000), *dmc1⁺* could have a function in unexpected cell cycle progression which is unrelated to recombination.

The meiotic delay observed in *dmc1Δ* cells is not dependent on checkpoint *rad* genes (*rad17⁺*, *rad3⁺*, *rad1⁺* and *rad9⁺*); however, *rad17⁺* is required for maintenance of viable spores and meiotic recombination frequency in *dmc1Δ* cells (Figure 2). One possible explanation of this phenotype is that *dmc1⁺* and *rad17⁺* might have a function in recombination between homologous chromosomes in an independent way. Thus, when both genes are defective, meiotic recombination between homologous chromosomes would strongly decrease, resulting in reduced spore viability. Further examination of Dmc1 function should provide new insights into the regulatory mechanism of meiotic progression.

Materials and methods

Yeast strains, media and genetic methods

The *S.pombe* strains used in this study are listed in Table I. Standard *S.pombe* genetic procedures were followed (Moreno *et al.*, 1991). Complete media YPD or YE containing adenine sulfate (75 μg/ml), synthetic minimal medium EMM2, sporulation medium ME or EMM2-N and germination media YEAde or EMMG were used. The homozygous diploid strains were constructed by cell fusion.

Spore viability and recombination assays

Haploid parental strains were grown on YPD plates at 33°C, cultured in YE-Ade and harvested at the stationary phase. Cells were mated and sporulated on ME plates at 28°C (zygotic meiosis). After 3–4 days of incubation, spores were treated with 0.5% glusulase (NEN Life Science Products, Inc.) for 16 h at 36°C and checked microscopically for the complete digestion of contaminating vegetative cells. The glusulase-treated spores were washed with water and then used for the spore viability assay and the intragenic recombination assay.

Spore viability assays. A total of 160 spores were spotted with a micromanipulator (MS series 200; Singer Instrument, UK) on EMMG containing supplements and germinated at 30°C for 4 days. Colonies were counted and the spore viability was expressed as a percentage relative to the 160 spores. We repeated this assay three times for each strain.

Intragenic recombination assays. We determined recombination frequencies as described previously (Nabeshima *et al.*, 2001). To examine the frequency of intragenic recombination, we used two *ade6* alleles (*ade6-M26* and *ade6-469*) as the intragenic recombination between these alleles produces the *ade6⁺* allele.

Synchronous meiosis

Fresh homozygous *pat1-114* diploid strains were grown in EMM with supplements at 25°C for >24 h. Cells at the mid-log phase were collected, washed and then transferred at a density of 3–4 × 10⁶ cells/ml to EMM2 containing supplements Leu (60 μg/ml) and Ura (40 μg/ml) but lacking NH₄Cl. After 16 h of incubation at 25°C, NH₄Cl (5 mg/ml) and supplements Leu (250 μg/ml) and Ura (75 μg/ml) were added to the culture medium and then the temperature was raised to 34°C to induce meiosis. The progression of meiosis was monitored by staining the methanol-fixed cells with DAPI (Wako). For γ-ray analysis, horsetail cells (3 h after temperature shift) were irradiated from a ⁶⁰Co source at a dose rate of 468 Gy/h for ~20 min (170 Gy).

Meiotic DSB assays

The procedures for PFGE have been described previously (Cervantes *et al.*, 2000). Meiosis was induced in *pat1* diploid cells by shifting the temperature, and 14 ml of cultured cells were collected at the indicated times. PFGE was conducted in a 0.8% chromosomal grade agarose gel (Bio-Rad) in a Bio-Rad CHEF-Mapper system at 14°C for 48 h with 2 V/cm, 100°C-induced angle in 1× TAE buffer (40 mM Tris-acetate pH 8.0, 1 mM EDTA), with a switch time of 30 min.

2816

Table I. Strains used in this study

Strain	Genotype
MS111w1	*h⁺ ura4-D18 leu1-32 ade6-469 his2*
MS105-1B	*h⁻ ura4-D18 ade6-M26*
MS126-4	*h⁺ ura4-D18 leu1-32 ade6-469 his2 rad3::ura4⁺*
MS162-1	*h⁻ ura4-D18 ade6-M26 rad3::ura4⁺*
MS111-1	*h⁺ ura4-D18 leu1-32 ade6-469 his2 rad17::ura4⁺*
MS105-22D	*h⁻ ura4-D18 ade6-M26 rad17::ura4⁺*
MS203-2	*h⁺ ura4-D18 leu1-32 ade6-469 his2 mek1::ura4⁺*
MS202-11	*h⁻ ura4-D18 ade6-M26 mek1::ura4⁺*
MS233-4	*h⁺ ura4-D18 leu1-32 ade6-469 his2 cds1::ura4⁺*
MS245-3	*h⁻ ura4-D18 ade6-M26 cds1::ura4⁺*
MS111m13	*h⁺ ura4-D18 leu1-32 ade6-469 his2 meu13::ura4⁺*
MS105-22C	*h⁻ ura4-D18 ade6-M26 meu13::ura4⁺*
MS133-1	*h⁺ ura4-D18 leu1-32 ade6-469 his2 dmc1::ura4⁺*
MS114-3	*h⁻ ura4-D18 ade6-M26 dmc1::ura4⁺*
MS128-15	*h⁺ ura4-D18 leu1-32 ade6-469 his2 rad3::ura4⁺ meu13::ura4⁺*
MS163-10	*h⁻ ura4-D18 ade6-M26 rad3::ura4⁺ meu13::ura4⁺*
MS111-6	*h⁺ ura4-D18 leu1-32 ade6-469 his2 rad17::ura4⁺ meu13::ura4⁺*
MS105-25C	*h⁻ ura4-D18 ade6-M26 rad17::ura4⁺ meu13::ura4⁺*
MS203-2	*h⁺ ura4-D18 leu1-32 ade6-469 his2 mek1::ura4⁺ meu13::ura4⁺*
MS202-10	*h⁻ ura4-D18 ade6-M26 mek1::ura4⁺ meu13::ura4⁺*
MS233-3	*h⁺ ura4-D18 leu1-32 ade6-469 his2 cds1::ura4⁺ meu13::ura4⁺*
MS245-7	*h⁻ ura4-D18 ade6-M26 cds1::ura4⁺ meu13::ura4⁺*
MS133-1	*h⁺ ura4-D18 leu1-32 ade6-469 his2 rad17::ura4⁺ dmc1::ura4⁺*
MS114-3	*h⁻ ura4-D18 ade6-M26 rad17::ura4⁺ dmc1::ura4⁺*
JZ670ᵃ	*h⁻/h⁻ pat1-114/pat1-114 leu1-32/ leu1-32 ade6-M210/ade6-M216*
KN8	*h⁻/h⁻ pat1-114/pat1-114 ura4-D18/ ura4-D18 leu1-32/ leu1-32 ade6-M210/ade6-M216 meu13::ura4⁺/meu13::ura4⁺*
MS276-1	*h⁻/h⁻ pat1-114/pat1-114 ura4-D18/ ura4-D18 leu1-32/ leu1-32 ade6-M210/ade6-M216 dmc1::ura4⁺/dmc1::ura4⁺*
MS123-5	*h⁻/h⁻ pat1-114/pat1-114 ura4-D18/ ura4-D18 leu1-32/ leu1-32 ade6-M210/ade6-M216 rec12::LEU2/ rec12::LEU2*
MS110-2	*h⁻/h⁻ pat1-114/pat1-114 ura4-D18/ ura4-D18 leu1-32/ leu1-32 ade6-M210/ade6-M216 rec12::LEU2/rec12::LEU2 meu13::ura4⁺/meu13::ura4⁺*
MS189-1	*h⁻/h⁻ pat1-114/pat1-114 ura4-D18/ ura4-D18 leu1-32/ leu1-32 ade6-M210/ade6-M216 rec12::LEU2/rec12::LEU2 dmc1::ura4⁺/dmc1::ura4⁺*
MS101-4	*h⁻/h⁻ pat1-114/pat1-114 ura4-D18/ ura4-D18 leu1-32/ leu1-32 ade6-M210/ade6-M216 rad17::ura4⁺/rad17::ura4⁺*
MS107-1	*h⁻/h⁻ pat1-114/pat1-114 ura4-D18/ ura4-D18 leu1-32/ leu1-32 ade6-M210/ade6-M216 rad17::ura4⁺/rad17::ura4⁺ meu13::ura4⁺/meu13::ura4⁺*
MS190-7	*h⁻/h⁻ pat1-114/pat1-114 ura4-D18/ ura4-D18 leu1-32/ leu1-32 ade6-M210/ade6-M216 rad17::ura4⁺/rad17::ura4⁺ dmc1::ura4⁺/dmc1::ura4⁺*
MS231-1	*h⁻/h⁻ pat1-114/pat1-114 ura4-D18/ ura4-D18 leu1-32/ leu1-32 ade6-M210/ade6-M216 cds1::ura4⁺/cds1::ura4⁺ meu13::ura4⁺/meu13::ura4⁺*
MS217-1	*h⁻/h⁻ pat1-114/pat1-114 ura4-D18/ ura4-D18 leu1-32/ leu1-32 ade6-M210/ade6-M216 mek1::ura4⁺/mek1::ura4⁺ meu13::ura4⁺/meu13::ura4⁺*
MS197-6	*h⁻/h⁻ pat1-114/pat1-114 ura4-D18/ ura4-D18 leu1-32/ leu1-32 ade6-M210/ade6-M216 Cds1:2HA: ura4⁺/Cds1*
MS198-1	*h⁻/h⁻ pat1-114/pat1-114 ura4-D18/ ura4-D18 leu1-32/ leu1-32 ade6-M210/ade6-M216 meu13::ura4⁺/meu13::ura4⁺ Cds1:2HA: ura4⁺/Cds1*
MS108-1	*h⁻/h⁻ pat1-114/pat1-114 ura4-D18/ ura4-D18 leu1-32/ leu1-32 ade6-M210/ade6-M216 Chk1:3HA/Chk1*
MS196-2	*h⁻/h⁻ pat1-114/pat1-114 ura4-D18/ ura4-D18 leu1-32/ leu1-32 ade6-M210/ade6-M216 meu13::ura4⁺/meu13::ura4⁺ Chk1:3HA/Chk1*
MS199-4	*h⁻/h⁻ pat1-114/pat1-114 ura4-D18/ ura4-D18 leu1-32/ leu1-32 ade6-M210/ade6-M216 Mek1:3HA:LEU2/Mek1*
MS200-5	*h⁻/h⁻ pat1-114/pat1-114 ura4-D18/ ura4-D18 leu1-32/ leu1-32 ade6-M210/ade6-M216 meu13::ura4⁺/meu13::ura4⁺ Mek1:3HA:LEU2/Mek1*
TP4-1D	*h⁺ ura4-D18 leu1-32 ade6-M216 his2*
TP4-5A	*h⁻ ura4-D18 leu1-32 ade6-M210*

ᵃProvided by M.Yamamoto.

Protein extraction and western blotting

Protein extracts were prepared as described previously (Caspari *et al.*, 2000) and western blots were performed as published (Shimada *et al.*, 1999). For the detection of Cds1HA, Chk1HA and Mek1HA, the blots were probed with mouse monoclonal antibodies 12CA5 (Boehringer Mannheim for Chk1HA and Mek1HA) and 16B12 (COVANCE Inc. for Cds1HA), then stripped and reprobed with anti-tubulin antibody (Sigma T5168) as a loading control. For the detection of Cdc2 Tyr15 phosphorylation, the blots were probed with an anti-phospho-Cdc2 (Tyr15) rabbit polyclonal antibody (NEB 9111), then stripped and reprobed with the anti-Cdc2 antibody (Santa Cruz Biotechnology, Santa Cruz, CA).

Mek1 disruption

The *mek1⁺* gene was disrupted by replacing it with the *ura4⁺* gene. To do this, we performed PCR and obtained a DNA fragment carrying the 5′

upstream region and 3′ downstream region of the *mek1⁺* gene. For this purpose, we synthesized the following four oligonucleotides and used them as primers: mek1-5F, 5′-CGGGGTACCTGCAGAATTGAAAA-TACGTCAAACCGAAC-3; mek1-5R, 5′-CCGCTCGAGCACTTTG-CAAAACGGTGATGCGCGTAAGC-3′; mek1-3F, 5′-AAAACTG-CAGCTCGAGCCACGTAAGAAAATATTCCGATAAACTTG-3′; and mek1-3R, 5′-CCCGAGCTCTAATTTAATATATCTTTGCTTGAAT-TATCG-3′. The underlined sequences denote the artificially introduced restriction enzyme sites for *Kpn*I, *Xho*I, *Pst*I–*Xho*I and *Sac*I, respectively. These PCR products and the 1.8 kb *Hind*III fragment containing the *ura4⁺* gene (Grimm *et al.*, 1988) were inserted into the pBluescriptII KS(+) vector via the *Kpn*I–*Xho*I, *Pst*I–*Sac*I and *Hind*III sites, respectively. This plasmid construct was digested with *Kpn*I and *Sac*I and the resulting construct was introduced into the diploid strain TP4-5A/TP4-1D. The Ura⁺ transformants were then screened by Southern blot analysis to identify the disrupted strain.

2817

Construction of Mek1-3HA strain

To prepare the Mek1-3HA construct, we performed PCR and obtained a DNA fragment carrying the open reading frame (ORF) region and the 3′ downstream region of the *mek1⁺* gene. For this purpose, we synthesized the following four oligonucleotides and used them as primers: mek1-ORF-F, 5′-ATAGGCGCGCCGTCGACTATGGACTTTTTATCAC-ATGCCATGC-3′; and mek1-ORF-R, 5′-TATTCTTAGCGGCCGCCG-TAGCCGGGAATGTTTAAGAGG-3′. The underlined sequences denote the artificially introduced restriction enzyme sites for *AscI–SalI* and *NotI*, respectively. To obtain the 3′ downstream region, we used the same primers as described above. These PCR products were inserted into the pIL(II) vector (T.Nakamura, unpublished), which is designed to allow one-step integration via *SalI–NotI* and *XhoI–SacI* sites, respectively. This plasmid construct was digested with *MluI*. The resulting construct was introduced into the haploid strains TP4-5A and TP4-1D. We then screened the Leu⁺ transformants by Southern blot analysis to identify the Mek1-3HA tagged strain.

Acknowledgements

References

Bahler,J., Wyler,T., Loidl,J. and Kohli,J. (1993) Unusual nuclear structures in meiotic prophase of fission yeast: a cytological analysis. *J. Cell Biol.*, 121, 241–256.

Bishop,D.K., Park,D., Xu,L. and Kleckner,N. (1992) DMC1: a meiosis-specific yeast homolog of recA required for recombination, synaptonemal complex formation and cell cycle progression. *Cell*, 69, 439–456.

Caspari,T. and Carr,A.M. (1999) DNA structure checkpoint pathways in *Schizosaccharomyces pombe*. *Biochimie*, 81, 173–181.

Caspari,T., Dahlen,M., Kanter,S.G., Lindsay, HD., Hofmann,K., Papadimitriou,K., Sunnerhagen,P. and Carr,A.M. (2000) Characteriz-ation of *Schizosaccharomyces pombe* Hus1; a PCNA-related protein that associates with Rad1 and Rad9. *Mol. Cell. Biol.*, 20, 1254–1262.

Cervantes,M.D., Farah,J.A. and Smith,G.R. (2000) Meiotic DNA breaks associated with recombination in *S.pombe*. *Mol. Cell*, 5, 883–888.

Cha,R.S., Weiner,B.M., Keeney,S., Dekker,J. and Kleckner,N. (2000) Progression of meiotic DNA replication is modulated by interchromosomal interaction proteins, negatively by SPO11p and positively by Rec8p. *Genes Dev.*, 14, 493–503.

Fukushima,K., Tanaka,Y., Nabeshima,K., Yoneki,T., Tougan,T., Tanaka,S. and Nojima,H. (2000) Dmc1 of *Schizosaccharomyces pombe* plays a role in meiotic recombination. *Nucleic Acids Res.*, 28, 2709–2716.

Grimm,C., Kohli,J., Murray,J. and Maundrell,K. (1988) Genetic engineering of *Schizosaccharomyces pombe*: a system for gene disruption and replacement using the *ura4* gene as a selectable marker. *Mol. Gen. Genet.*, 215, 81–86.

Hartwell,L.H. and Weinert,T.A. (1989) Checkpoints: controls that ensure the order of cell cycle events. *Science*, 246, 629–634.

Hunter,N. and Kleckner,N. (2001) The single-end invasion: an asymmetric intermediate at the double-strand break to double-Holliday junction transition of meiotic recombination. *Cell*, 106, 59–70.

Iino,Y. and Yamamoto,M. (1985) Mutants of *Schizosaccharomyces pombe* which sporulate in the haploid state. *Mol. Gen. Genet.*, 198, 416–421.

Kato,R. and Ogawa,H. (1994) An essential gene, *ESR1*, is required for mitotic cell growth, DNA repair and meiotic recombination in *Saccharomyces cerevisiae*. *Nucleic Acids Res.*, 22, 3104–3112.

Kleckner,N. (1996) Meiosis: how could it work? *Proc. Natl Acad. Sci. USA*, 93, 8167–8174.

Leu,J.Y. and Roeder,G.S. (1999) The pachytene checkpoint in *S.cerevisiae* depends on Swe1-mediated phosphorylation of the cyclin-dependent kinase Cdc28. *Mol. Cell*, 4, 805–814.

Lydall,D., Nikolsky,Y., Bishop,D.K. and Weinert,T. (1996) A meiotic recombination checkpoint controlled by mitotic checkpoint genes. *Nature*, 383, 840–843.

Moreno,S., Klar,A. and Nurse,P. (1991) Molecular genetic analysis of fission yeast *Schizosaccharomyces pombe*. *Methods Enzymol.*, 194, 795–823.

Murakami,H. and Nurse,P. (1999) Meiotic DNA replication checkpoint control in fission yeast. *Genes Dev.*, 13, 2581–2593.

Nabeshima,K., Kakihara,Y., Hiraoka,Y. and Nojima,H. (2001) A novel meiosis-specific protein of fission yeast, Meu13p, promotes homologous pairing independently of homologous recombination. *EMBO J.*, 20, 3871–3881.

Rhind,N. and Russell,P. (1998) Tyrosine phosphorylation of cdc2 is required for the replication checkpoint in *Schizosaccharomyces pombe*. *Mol. Cell. Biol.*, 18, 3782–3787.

Rhind,N., Furnari,B. and Russell,P. (1997) Cdc2 tyrosine phosphoryl-ation is required for the DNA damage checkpoint in fission yeast. *Genes Dev.*, 11, 504–511.

Rockmill,B. and Roeder,G.S. (1991) A meiosis-specific protein kinase homolog required for chromosome synapsis and recombination. *Genes Dev.*, 5, 2392–2404.

Roeder,G.S. (1997) Meiotic chromosomes: it takes two to tango. *Genes Dev.*, 11, 2600–2621.

Roeder,G.S. and Bailis,J.M. (2000) The pachytene checkpoint. *Trends Genet.*, 16, 395–403.

Shimada,M., Okuzaki,D., Tanaka,S., Tougan,T., Tamai,K.K., Shimoda,C. and Nojima,H. (1999) Replication factor C3 of *Schizosaccharomyces pombe*, a small subunit of replication factor C complex, plays a role in both replication and damage checkpoints. *Mol. Biol. Cell*, 10, 3991–4003.

Stuart,D. and Wittenberg,C. (1998) CLB5 and CLB6 are required for premeiotic DNA replication and activation of the meiotic S/M checkpoint. *Genes Dev.*, 12, 2698–2710.

Tung,K.S., Hong,E.J. and Roeder,G.S. (2000) The pachytene checkpoint prevents accumulation and phosphorylation of the meiosis-specific transcription factor Ndt80. *Proc. Natl Acad. Sci. USA*, 97, 12187–12192.

Watanabe,T., Miyashita,K., Saito,T.T., Yoneki,T., Kakihara,Y., Nabeshima,K., Kishi,Y.A., Shimoda,C. and Nojima,H. (2001) Comprehensive isolation of meiosis-specific genes identifies novel proteins and unusual non-coding transcripts in *Schizosaccharomyces pombe*. *Nucleic Acids Res.*, 29, 2327–2337.

Xu,L., Weiner,B.M. and Kleckner,N. (1997) Meiotic cells monitor the status of the interhomolog recombination complex. *Genes Dev.*, 11, 106–118.

2818

Cyclin G1 associates with MDM2 and regulates accumulation and degradation of p53 protein

Shinya H. Kimura[1,2] and Hiroshi Nojima[1,*]

[1]*Department of Molecular Genetics, Research Institute for Microbial Diseases, Osaka University, 3-1 Yamadaoka, Suita, Osaka 565-0871, Japan*
[2]*Department of Pharmacology, Hyogo College of Medicine, 1-1 Mukogawa-cho, Nishinomiya, Hyogo 663-8501, Japan*

Abstract

Background: Cyclin G1 is a transcriptional target of p53 and is induced by DNA damage in a p53 dependent manner. Analysis of cyclin G1 disrupted mice demonstrated that cyclin G1 is involved in many of the functions regulated by p53 such as apoptosis, growth control and check point regulation in response to DNA damage. The results suggest that the main role of cyclin G1 is to mediate or regulate the function of p53.

Results: Western blot analysis revealed that the accumulation of p53 protein during the initial 24 h period following DNA damage is reduced in cyclin $G1^{-/-}$ cells compared to wild-type cells. This decrease in p53 accumulation could be recovered by introducing a cDNA expressing cyclin G1. Cyclin G1 interacted directly with MDM2 and promoted the formation of the ARF/MDM2 complex within the initial 24 h period following DNA damage. Furthermore, 48 h after irradiation, accumulation of p53 protein was enhanced in cyclin $G1^{-/-}$ cells compared to wild-type cells. In contrast, in 48 h postirradiated wild-type cells, the cyclin G1-MDM2 complex was found not to be associated with ARF but with the $B'\alpha$ subunit of protein phosphatase A.

Conclusion: These results suggest that cyclin G1 stabilizes and promotes the degradation of p53 protein by associating, respectively, with MDM2 complexes containing ARF and PP2A.

Introduction

Cyclins have a highly conserved motif called the 'cyclin box', which consists of a 100-amino acid motif which is conserved between all cyclins (Nugent *et al.* 1991). Some cyclins associate with cyclin-dependent-kinases (cdks) via the cyclin box, and control cell cycle progression by functioning as the regulatory subunits of cdks that phosphorylate cellular substrates (Hunt 1991; Pines 1991). Cyclin G1 was originally identified as a novel member of the cyclin family (Tamura *et al.* 1993), and cyclin G2 was isolated as a homologue of cyclin G1 (Horne *et al.* 1996; Bates *et al.* 1996). Cyclin I may also belong to the cyclin G subfamily because of its high sequence homology to cyclin G1 and cyclin G2 (Nakamura *et al.* 1995; Bates *et al.* 1996).

Cyclin G1 is one of the target genes of the transcription factor p53 (Okamoto & Beach 1994; Zauberman

et al. 1995). The p53 tumour suppressor gene is involved in diverse cellular processes, including regulation of the cell cycle, apoptosis, senescence, DNA repair, cell differentiation and angiogenesis. The increase in p53 protein levels which occurs in response to genotoxic stress is thought to result in the transcription of target genes that mediate the varied functions associated with the p53 gene. Among the gene products of these transcriptional target genes, MDM2 (HDM2 in human) is a negative regulator of p53 (Barak *et al.* 1993; Wu *et al.* 1993), $p21^{WAF1/Cip1}$ is an inhibitor of cyclin-CDK complexes, whose inhibition results in G1 arrest (reviewed in El-Deiry 1998), GADD45 is involved in DNA repair (Smith *et al.* 1994), 14-3-3σ mediates G2 arrest (Hermeking *et al.* 1997), Bax promotes apoptosis (Miyashita & Reed 1995), and thrombospondin-1 inhibits angiogenesis (Dameron *et al.* 1994). Therefore, it seems likely that cyclin G1, which is also a transcriptional target of p53, may also act as a mediator of p53 functions such as growth inhibition, DNA repair and apoptosis, or may play a role in the regulation of p53 like MDM2.

Communicated by: Shunsuke Ishii
Correspondence: E-mail: hnojima@biken.osaka-u.ac.jp

Stabilization and activation of p53 protein in response to DNA damage depends upon protein kinases such as ATM (ataxia telangiectasia mutated) and ATR (ATM related). These kinases act directly by activating p53 through the phosphorylation of serine-15 (Shieh et al. 1997; Tibbetts et al. 1999; Unger et al. 1999; Chehab et al. 2000). It was reported that ATM or ATR also affects p53 indirectly via the downstream protein kinases Chk1 and Chk2, which stabilize p53 by directly phosphorylating p53 at serine-20 (Unger et al. 1999; Shieh et al. 1999, 2000; Hirao et al. 2000). Serine 20 of p53 lies within the MDM2–p53 interaction domain and its phosphorylation disturbs the association of p53 with MDM2 (Chehab et al. 1999; Unger et al. 1999).

During the process of p53 induction or stabilization, inhibition of its degradation, which is regulated by the ubiquitin-proteasome pathway, is important (Maki et al. 1996). MDM2 has intrinsic E3 ligase activity and conjugates ubiquitin to p53 (Honda et al. 1997; Honda & Yasuda 1999). MDM2 may also play a role in shuttling p53 from the nucleus to the cytoplasm to degrade p53 in cytoplasmic proteasomes (Freedman & Levine 1998; Roth et al. 1998; Tao & Levine 1999). These functions of MDM2 are inhibited by ARF, a 19 kDa protein in mouse (p19ARF) and a 14 kDa protein in human (p14ARF) (Kamijo et al. 1998; Pomerantz et al. 1998; Stott et al. 1998; Zhang et al. 1998). ARF, but not p53, associates with MDM2 and sequesters it into the nucleolus, thereby preventing negative-feedback regulation of p53 by MDM2 and leading to the activation of p53 in the nucleoplasm (Zhang et al. 1998; Honda & Yasuda 1999; Weber et al. 1999).

Cyclin G1 and cyclin G2 have been demonstrated to play an important role in some biological phenomena (Bates et al. 1996; Horne et al. 1997; Okamoto & Prives 1999) such as apoptosis (Reimer et al. 1999), and the molecules that they associate with have been identified (Okamoto et al. 1996; Kanaoka et al. 1997; Kimura et al. 1997). However, the precise functions of cyclin G1 and G2 remain unclear. In order to investigate the physiological role of cyclin G1, we generated mice homozygous for a targeted disruption of the cyclin G1 gene (Kimura et al. 2001). Our results demonstrated that cyclin G1 is involved in the multiple functions of p53 such as G2/M arrest and check point regulation in response to DNA damage (Kimura et al. 2001). The results suggested that cyclin G1 might perform its main role by mediating the function of p53, or by regulating p53 activation. Here, we report that the accumulation of p53 protein in response to DNA damage is remarkably reduced in cyclin G1$^{-/-}$ cells compared to wild-type cells, and that the MDM2-ARF complex associates with either cyclin G1

or cyclin G2 separately. These results provide a novel role for cyclin G1 and cyclin G2 in the MDM2–ARF interaction and in the subsequent stabilization of p53 protein.

Results

Accumulation of p53 protein is reduced in cyclin G1$^{-/-}$ cells between 6 h and 24 h following DNA damage

In order to identify the physiological role of cyclin G1, we have previously generated and characterized a cyclin G1-null mouse (Kimura et al. 2001). Cyclin G1$^{-/-}$ MEFs (mouse embryonic fibroblasts) derived from these mice showed a growth retardation, an abnormality in G2/M arrest and a decreased survival rate in response to DNA damage (Kimura et al. 2001). This result suggested that cyclin G1 could act by mediating the function of p53, or by regulating p53 activation. We investigated the profiles of p53 induction and its accumulation in wild-type and cyclin G1$^{-/-}$ cells in response to DNA damage induced by γ- or UV irradiation by Western blotting with anti-p53 antibody (Fig. 1A and B). In wild-type MEFs, we found that levels of p53 protein increased during the initial 3 h period following DNA damage, and then accumulated between 6 and 24 h (Fig. 1A and B). In cyclin G1$^{-/-}$ MEFs, a similar level of induction was observed up to 3 h, but the accumulation of p53 between 6 and 24 h was not observed (Fig. 1A and B). Recovery of the loss of accumulation of p53 between 6 and 24 h following γ-irradiation in cyclin G1$^{-/-}$ MEFs could be achieved by expression of cyclin G1 and G2 in the cells by transforming them with a retrovirus vector carrying cyclin G1 (Fig. 1C) or cyclin G2 (data not shown). These results indicate that cyclin G1 is involved in the stabilization of p53 protein and that cyclin G2 could compensate for a defect in cyclin G1 by stabilizing p53 protein.

Cyclin G1 plays a role in p53 accumulation via an ATM-independent pathway

It has previously been reported that the stabilization and activation of p53 protein in response to DNA damage depends upon the protein kinases, ATM or ATR (ATM related). These kinases act directly by activating p53 through phosphorylation at serine-15 (Tibbetts et al. 1999; Shieh et al. 1997; Unger et al. 1999; Chehab et al. 2000). ATM or ATR also affect p53 indirectly via the downstream protein kinases Chk1 and Chk2, which stabilize p53 by a direct phosphorylation of p53 at serine-20 (Unger et al. 1999; Shieh et al. 1999, 2000; Hirao et al. 2000). This demonstrated a role for the AT-Chk
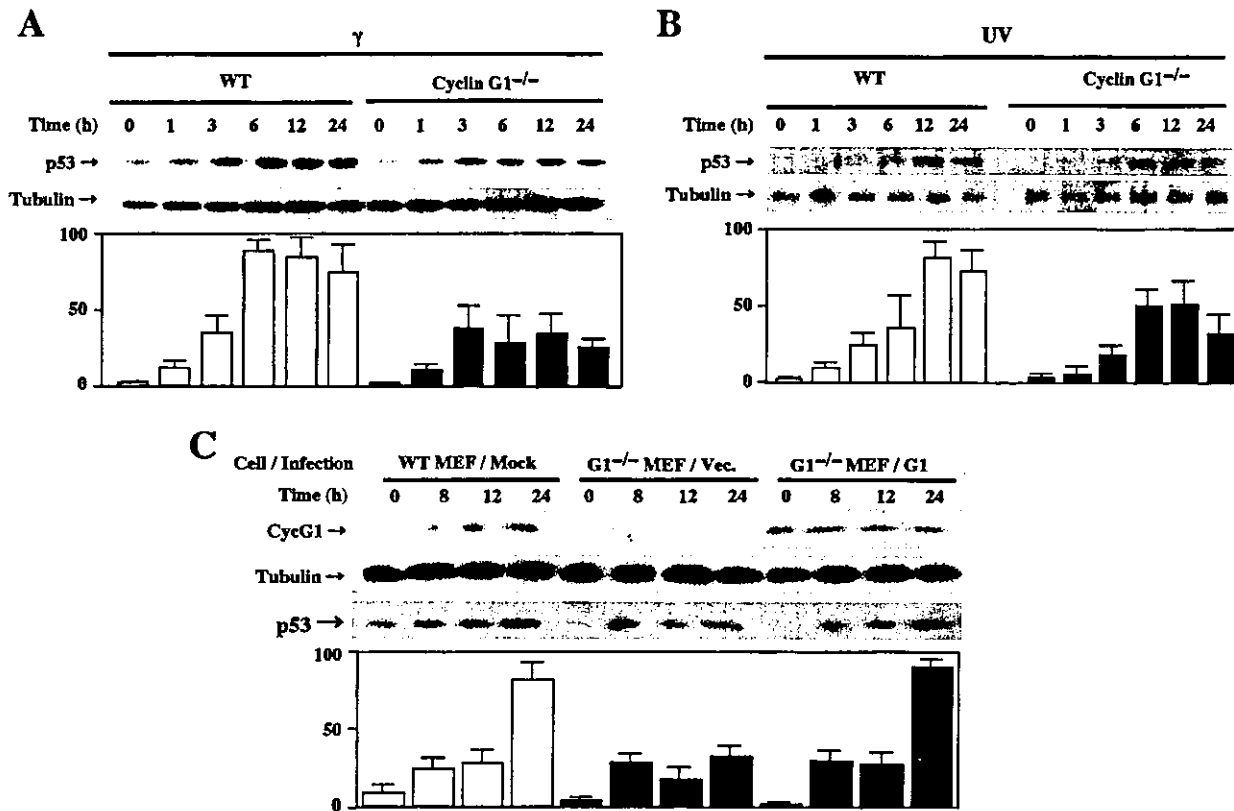
Figure 1 Decrease in p53-accumulation in cyclin G1$^{-/-}$ cells in response to DNA damage. Mouse embryonic fibroblasts (MEFs) derived from wild-type and cyclin G1$^{-/-}$ mice were irradiated with 10 Gy of γ- (A) or 10 J/m^2 of UV-radiation (B). The lysates of these cells were then collected at the indicated times following irradiation and subjected to SDS-PAGE and Western blot analysis using anti-p53 antibody (upper panel). The same samples were probed with anti-tubulin antibody as a loading control (lower panel). Columns in the lower panel indicate the relative intensity of the p53 bands after correction for variation in the intensity of tubulin bands. Open and filled columns indicate the protein level in wild-type and cyclin G1$^{-/-}$ MEFs, respectively. Each value shows the mean of three experiments, and the bars represent standard errors. (C) Exogeneous cyclin G1 stabilizes and causes the accumulation of p53 protein in cyclin G1$^{-/-}$ MEFs. Cyclin G1$^{-/-}$ MEFs (G1$^{-/-}$ MEF) were infected 2 days before irradiation with retrovirus containing cyclin G1, cyclin G2 or an empty vector, as indicated at the top of the figure (Genotype/Construct). Wild-type MEFs were mock treated as a control. Cells were γ-irradiated (10 Gy), harvested at indicated time, lysed and subjected to SDS-PAGE and Western blot analysis to determine the level of p53, cyclin G1, cyclin G2 and tubulin expression. Columns in the lower panel indicated the relative intensity of the p53 bands after correction for loading variation by using the intensity of tubulin bands. Each value shows the mean of three experiments and bars represent standard errors.

pathway in stabilizing p53, and our evidence suggesting a role for cyclin G1 in p53 stabilization led us to further investigate the involvement of cyclin G1 in the process of p53 stabilization (Fig. 2A). Wortmannin, an inhibitor of the PI3-K family (Wymann et al. 1996), inhibits ATM activity and radiation-induced p53 accumulation (Yih & Lee 2000). When wild-type and cyclin G1$^{-/-}$ MEFs were treated with wortmannin and irradiated, p53 accumulation was inhibited in both cell types (Fig. 2A). This result indicates that a lack of functional cyclin G1 and an inhibition of AT kinase cumulatively affects p53 accumulation, suggesting that cyclin G1 and AT kinase affect p53 accumulation through independent pathways.

Inhibition of interaction between ARF and MDM2 in cyclin G1$^{-/-}$ MEFs

Nucleolar localization of MDM2 by ARF stabilizes p53 protein and protects it from ubiquitin-mediated degradation (Weber et al. 1999; Honda & Yasuda 1999; Zhang et al. 1998). We have immunoprecipitated cyclin G1, MDM2 and ARF in irradiated wild-type and cyclin G1$^{-/-}$ MEFs and have found that cyclin G1 co-precipitates with MDM2 and ARF in wild-type MEFs, whereas the co-precipitation of ARF and MDM2 was dramatically decreased in cyclin G1$^{-/-}$ MEFs (Fig. 2B). This result suggests that disruption of cyclin G1 inhibited the
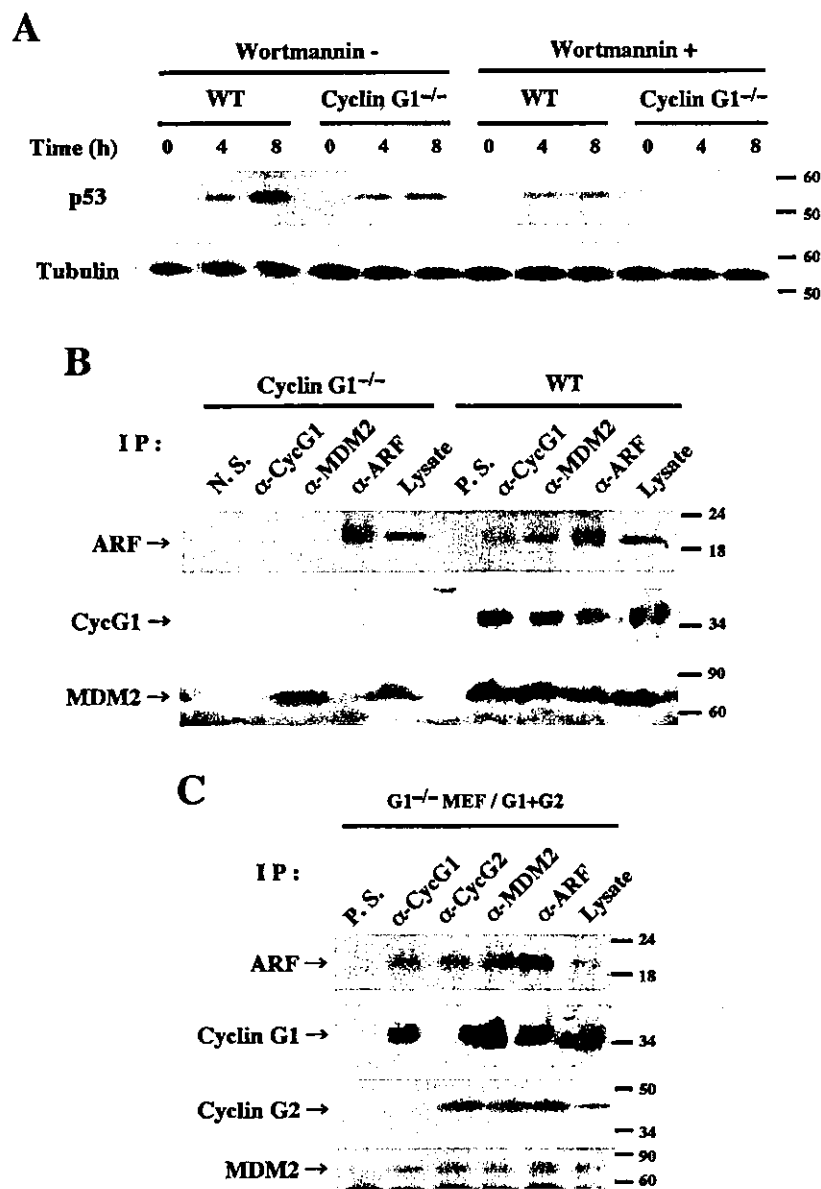
A

B

C

Figure 2 Cyclin G1 is not involved in the AT pathway, but rather regulates ARF to promote p53 accumulation in response to DNA damage. (A) Effect of wortmannin, an inhibitor of ATM kinase, on p53 accumulation in wild-type and cyclin G1$^{-/-}$ MEFs. Cells with or without 20 μM wortmannin treatment were irradiated with 10 Gy of γ-rays and harvested for Western blot analysis using either anti-p53 (upper panel) or anti-tubulin (lower panel) antibodies. (B) Association of cyclin G1 with MDM2 and ARF in wild-type MEFs, and loss of the association between MDM2 and ARF in cyclin G1$^{-/-}$ MEFs. MEFs were irradiated with 10 Gy of γ-rays and harvested 24 h after irradiation for immunoprecipitation with non-immune serum (N.S.), anti-ARF, anti-MDM2 or anti-cyclin G1 antibodies. Lysates and precipitates were then subjected to Western blot analysis using either anti-ARF (upper panel), anti-cyclin G1 (middle panel) or anti-MDM2 (lower panel) antibodies. (C) Association of cyclin G1 and cyclin G2 with the MDM2-ARF complex. Cyclin G1$^{-/-}$ MEFs were infected 2 days before irradiation with the retroviral constructs pBabePuro-cyclin G1 and pBabePuro-cyclin G2, and then irradiated with 10 Gy of γ-rays and harvested 24 h after irradiation for immunoprecipitation with the relevant antibodies. Precipitates and lysates were then subjected to Western blot analysis with anti-ARF (upper panel), anti-cyclin G1 (middle panel) or anti-cyclin G2 (lower panel) antibodies.

association of ARF with MDM2, and that cyclin G1 may regulate the interaction of MDM2 with ARF and their co-localization to the nucleolus. Using the same blot, we could not detect any cyclin G2 that co-precipitated, probably because of the low affinity of the anti-cyclin G2 antibody we used (data not shown). However, when cyclin G1$^{-/-}$ MEFs exogeneously expressing cyclin G1 and cyclin G2 were irradiated, we observed that cyclin G1 and cyclin G2 formed complexes with ARF and MDM2 (Fig. 2C). This result indicates that the MDM2-ARF complex can associate with either cyclin G1 or cyclin G2.

Cyclin G1 directly interacts with MDM2 *in vitro*

Immunoprecipitation experiments showed that cyclin G1 could be co-precipitated with MDM2 and ARF from the cell extracts of wild-type MEFs (Fig. 2B). In order to detect the association of cyclin G1 with MDM2 and/or ARF, we carried out *in vitro* pull down assays. For this experiment, GST and GST-cyclin G1 fusion proteins were expressed in *E. coli*, lysed, purified with glutathione-Sepharose beads, and subjected to SDS-PAGE. Western blotting demonstrated that GST and GST-cyclin G1 fusion proteins had been successfully
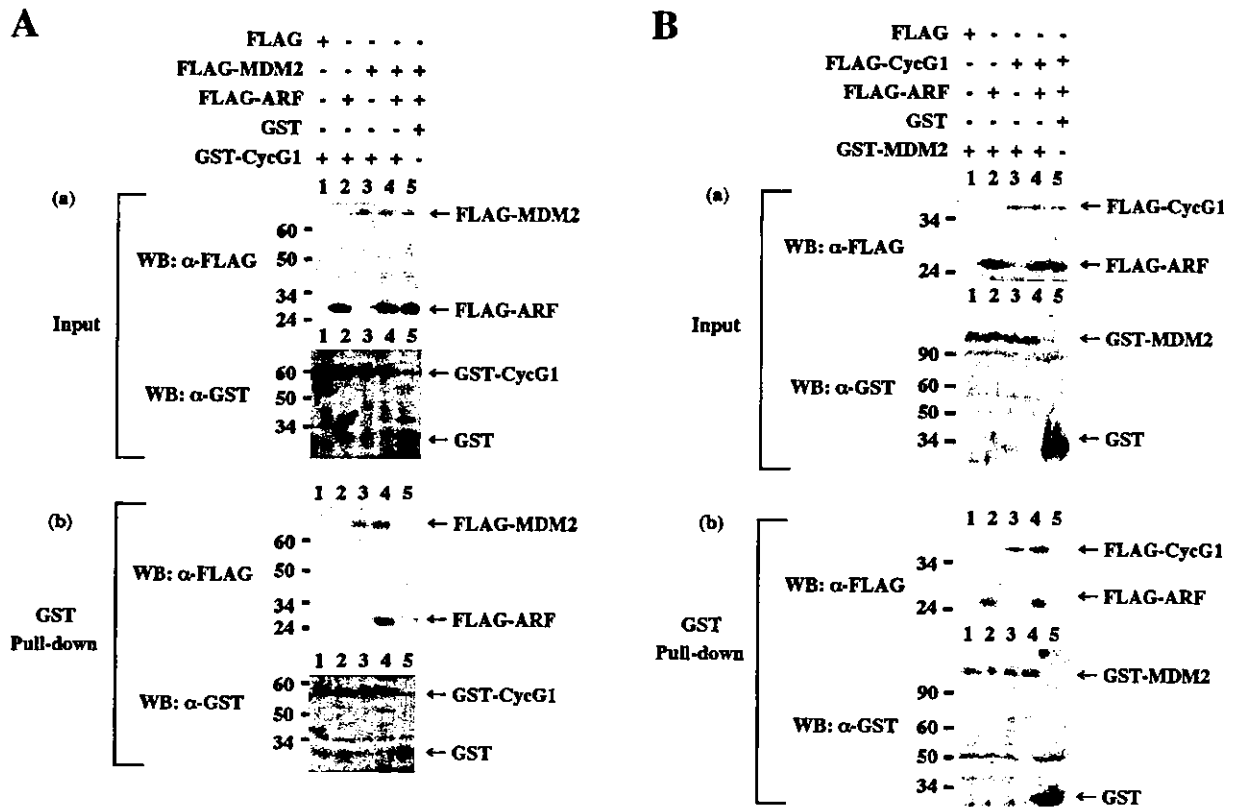
—364—

A

```
          FLAG  +  ·  ·  ·  ·
     FLAG-MDM2  ·  ·  +  +  +
      FLAG-ARF  ·  +  ·  +  +
           GST  ·  ·  ·  ·  +
     GST-CycG1  +  +  +  +  ·
                1  2  3  4  5
```

(a)

Input

WB: α-FLAG
60 – ← FLAG-MDM2
50 –
34 –
24 – ← FLAG-ARF

WB: α-GST
60 – ← GST-CycG1
50 –
34 – ← GST

(b)

GST Pull-down

WB: α-FLAG
60 – ← FLAG-MDM2
50 –
34 –
24 – ← FLAG-ARF

WB: α-GST
60 – ← GST-CycG1
50 –
34 – ← GST

B

```
          FLAG  +  ·  ·  ·  ·
    FLAG-CycG1  ·  ·  +  +  +
      FLAG-ARF  ·  +  ·  +  +
           GST  ·  ·  ·  ·  +
     GST-MDM2  +  +  +  +  ·
                1  2  3  4  5
```

(a)

Input

WB: α-FLAG
34 – ← FLAG-CycG1
24 – ← FLAG-ARF

WB: α-GST
90 – ← GST-MDM2
60 –
50 –
34 – ← GST

(b)

GST Pull-down

WB: α-FLAG
34 – ← FLAG-CycG1
24 – ← FLAG-ARF

WB: α-GST
90 – ← GST-MDM2
60 –
50 –
34 – ← GST

Figure 3 Cyclin G1 associates with MDM2 *in vitro*. (A) Glutathione Sepharose beads bound to GST-cyclin G1 fusion protein was added to the lysate mixtures containing the indicated FLAG-fusion protein and used in the pull down experiments. *E. coli* lysates expressing GST alone, GST-cyclin G1, and FLAG-fusion proteins (a), and precipitated proteins (b) were subjected to SDS-PAGE and Western blotting with anti-FLAG or anti-GST monoclonal antibody. (B) GST-MDM2 fusion protein was added to the lysate mixture containing the indicated FLAG-fusion proteins and used in the pull down experiments. *E. coli* lysates expressing GST alone, GST-cyclin G1, and FLAG-fusion proteins (a), and precipitated proteins (b) were subjected to SDS-PAGE and Western blotting with anti-FLAG or anti-GST monoclonal antibody.

purified from the cell extracts by the glutathione-Sepharose beads (Fig. 3Aa, lower panel). ARF and MDM2 genes were fused to the FLAG tag and expressed in *E. coli*. The lysates containing FLAG-fusion proteins were mixed with each other as indicated in Fig. 3A, and used for the pull down assay. Western blotting of these lysates revealed that the FLAG-MDM2 and FLAG-ARF were successfully expressed (Fig. 3A,a, upper panel). Beads containing bound GST-fusion proteins were added to the lysate (lanes 1, 2 and 3) or lysate mixtures (lanes 4 and 5) containing each of the FLAG-fusion proteins, washed with IP buffer, and precipitated. Precipitates were then analysed by Western blotting with anti-FLAG antibody (Fig. 3Ab, upper panel). As shown in Fig. 3Ab, the FLAG-MDM2 band was detected by FLAG M2 antibody in all of the lanes precipitated with GST-cyclin G1 (Fig. 3Ab, lanes 3 and 4). The interaction of GST-cyclin G1 with MDM2 was detected even in the absence of

ARF (Fig. 3Ab, lane 3), whereas the interaction of GST-cyclin G1 with ARF could not be detected in the absence of MDM2 (Fig. 3Ab, lane 2). This result shows that cyclin G1 interacts directly with MDM2.

GST-MDM2 and FLAG-cyclin G1 were also constructed and used in reciprocal experiments. The expression of these proteins was confirmed by SDS-PAGE and Western blotting (Fig. 3Ba). Beads containing bound GST-fusion proteins were added to lysate mixtures containing each FLAG-fusion protein and the beads were precipitated and washed. Western blotting of the bead precipitates with anti-FLAG antibody allowed the detection of the interactions between these proteins. Lane 2 of Fig. 3Bb shows a direct interaction between GST-MDM2 and FLAG-ARF. This result is consistent with previous reports which demonstrated that MDM2 and ARF interact together *in vitro* and *in vivo* (Kamijo *et al.* 1998; Pomerantz *et al.* 1998; Stott *et al.* 1998; Tao

A

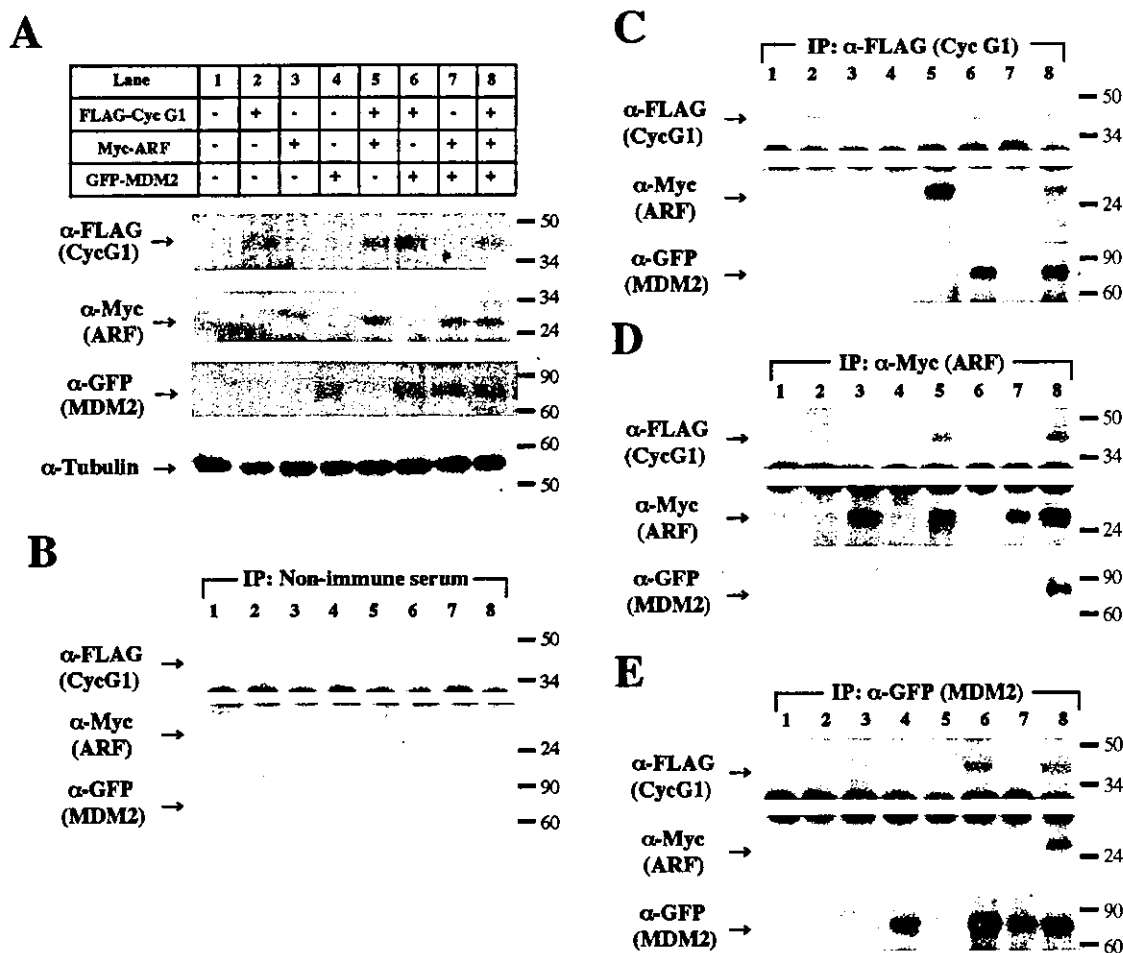| Lane	1	2	3	4	5	6	7	8
FLAG-Cyc G1	-	+	-	-	+	+	-	+
Myc-ARF	-	-	+	-	+	-	+	+
GFP-MDM2	-	-	-	+	-	+	+	+

B

C

D

E

Figure 4 Cyclin G1 associates with MDM2 and ARF and mediates their interaction. (A) Expression of FLAG-cyclin G1, Myc-ARF and GFP-MDM2 in 293T cells. Combinations of transfection vectors expressing FLAG-cyclin G1, Myc-ARF and/or GFP-MDM2 are shown. The expression vector DNAs were mixed together (shown as '+' in the figure) and transfected into 293T cells. Cells were harvested 48 h after transfection and subjected to Western blot analysis using anti-FLAG (upper panel), anti-Myc (the second panel) or anti-GFP (the third panel) to detect the expression of cyclin G1, ARF and MDM2, respectively. The same samples were also subjected to Western blot analysis using anti-tubulin antibody as a loading control (lower pane). (B–E) Detection of the interactions between cyclin G1, ARF and MDM2. Lysates analysed in (A) were used in immunoprecipitations using non-immune serum (B), anti-FLAG (C), anti-Myc (D) and anti-GFP (E) antibodies. Precipitates were then subjected to Western blot analysis using the relevant antibodies.

& Levine 1999; Weber et al. 1999, 2000; Zhang et al. 1998). In our experiments, GST-MDM2 directly associated with FLAG-cyclin G1 irrespective, of the presence or absence of FLAG-ARF (Fig. 3B, lanes 3 and 4).

Cyclin G1 promotes the formation of ARF/MDM2 complex

In order to confirm the association of cyclin G1 with MDM2 and ARF in vivo, expression vectors containing FLAG-tagged cyclin G1, Myc-tagged ARF and GFP-tagged MDM2 were introduced into 293T cells by lipofection. Western blot analysis on cellular lysates confirmed that these expression vectors had been successfully introduced into the cells and were expressing their respective proteins (Fig. 4A). These lysates were then used in immunoprecipitations with either non-immune serum (Fig. 4B), anti-FLAG (Fig. 4C), anti-Myc (Fig. 4D) or anti-GFP (Fig. 4E) antibody, respectively. These precipitates were then analysed by Western blotting with anti-FLAG, anti-Myc and anti-GFP antibodies to detect FLAG-cyclin G1 (Fig. 4B–E, upper panels), Myc-ARF (Fig. 4B–E, middle panels), and GFP-MDM2 (Fig. 4B–E, lower panels), respectively. An interaction between
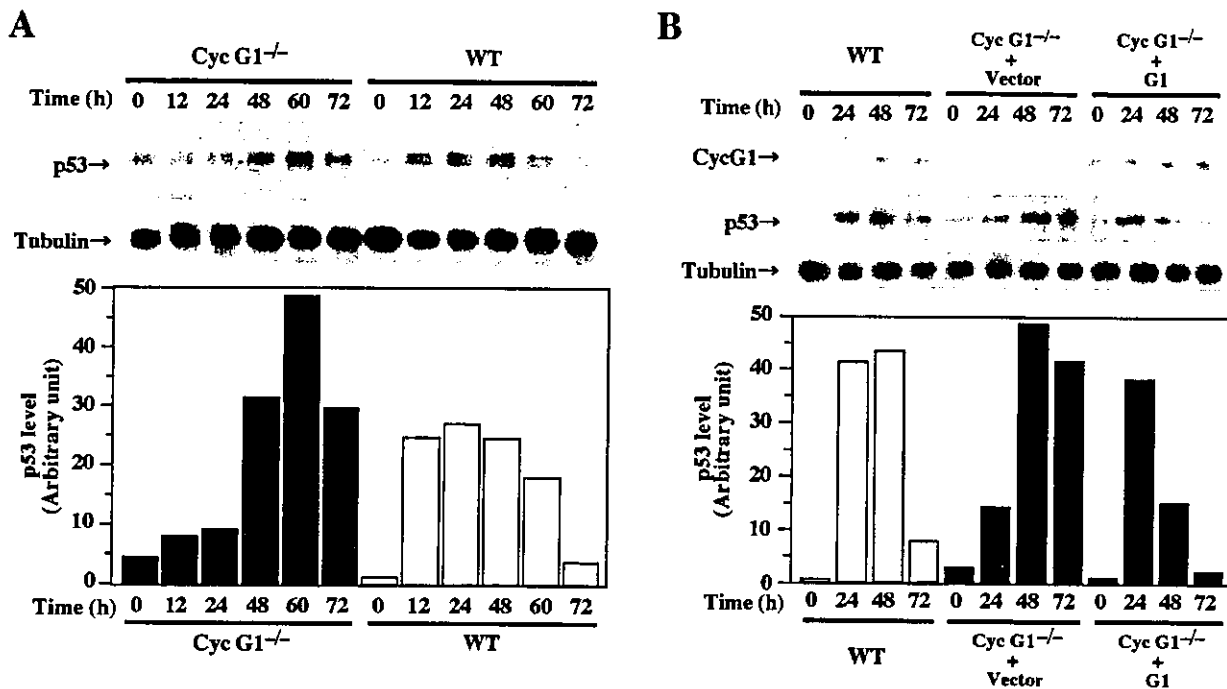
-366-

Figure 5 Enhancement of the p53 protein level in cyclin G1⁻/⁻ MEF in late period of recovery from DNA damage. (A) MEFs derived from wild-type and cyclin G1⁻/⁻ mice were irradiated with 10 Gy of γ-radiation. The lysates of these cells were then collected at the indicated times following irradiation and subjected to SDS-PAGE and Western blot analysis using anti-p53 antibody (upper panel). The same samples were probed with anti-tubulin antibody as a loading control (lower panel). Columns in the lower panel indicate the relative intensity of the p53 bands after correction for variations in the intensity of the tubulin bands. Open and filled columns indicate the protein level in wild-type and cyclin G1⁻/⁻ MEFs, respectively. (B) Exogeneous cyclin G1 corrects for the abnormal p53 level in cyclin G1⁻/⁻ MEFs. Cyclin G1⁻/⁻ MEFs (G1⁻/⁻ MEF) were infected with a retrovirus containing cyclin G1 or an empty vector as indicated at the top of the figure (Genotype + Construct). Wild-type MEFs were mock treated as a control. Cells were γ-irradiated (10 Gy) 48 h after infection, harvested at the indicated times, lysed and subjected to SDS-PAGE and Western blot analysis to determine the level of p53, cyclin G1, cyclin G2 and tubulin expression. Columns in the lower panel indicate the relative intensity of the p53 bands after correcting for loading variation by measuring the intensity of the tubulin bands.

MDM2 and ARF was not detected in the absence of cyclin G1 expression (Fig. 2D,E, lane 7), although cyclin G1 interacted with ARF without GFP-MDM2 expression (Fig. 2C,D, lane 5), and with MDM2 without Myc-ARF expression (Fig. 2C,E, lane 6). Co-precipitation of MDM2 and ARF was detected only when there was expression of cyclin G1, MDM2 and ARF (Fig. 2C–E, lane 8). These results suggest that cyclin G1 can associate independently with MDM2 or ARF, and that it promotes the formation of the MDM2/ARF complex.

Accumulation of p53 protein is up-regulated in cyclin G1⁻/⁻ cells 48 h after DNA damage

Figure 1 shows that the induction of p53 protein is down-regulated in 24 h post-irradiated cyclin G1⁻/⁻ MEFs and that cyclin G1 positively regulates p53 protein accumulation. Taking these results into account, it seems

reasonable to conclude that a decrease in the level of p53 protein accelerates the growth of cyclin G1⁻/⁻ MEFs in response to DNA damage. However, growth retardation of cyclin G1⁻/⁻ MEFs after DNA damage has been observed (Kimura et al. 2001). In order to confirm the reduced level of p53 in cyclin G1⁻/⁻ MEFs, we carried out a Western blot analysis on lysates from 24 h post-irradiated MEFs and wild-type cells (Fig. 5A). In these samples, the level of p53 on these lysates was greater in cyclin G1⁻/⁻ MEFs than in the wild-type cells. The results presented in Fig. 5A show that the level of p53 protein decreases initially within the 24 h post-irradiation period in cyclin G1⁻/⁻ MEFs, but increases thereafter to reach a level superior to that of wild-type MEFs.

In order to confirm that cyclin G1 up-regulates p53 protein within the 24 h post-irradiation period, we analysed cyclin G1⁻/⁻ MEF expressing exogeneous cyclin G1. Analyses of cyclin G1⁻/⁻ MEF expressing cyclin G1

A

Western blot

Time (h)	0	24	48	60
p53				
CycG1				
PP2AB'α				
MDM2				
ARF				
Tubulin				

B

IP : α-Cyclin G1

Time (h)	0	24	48	60
CycG1 →				
MDM2 →				
PP2A B'α →				
ARF →				

C

IP

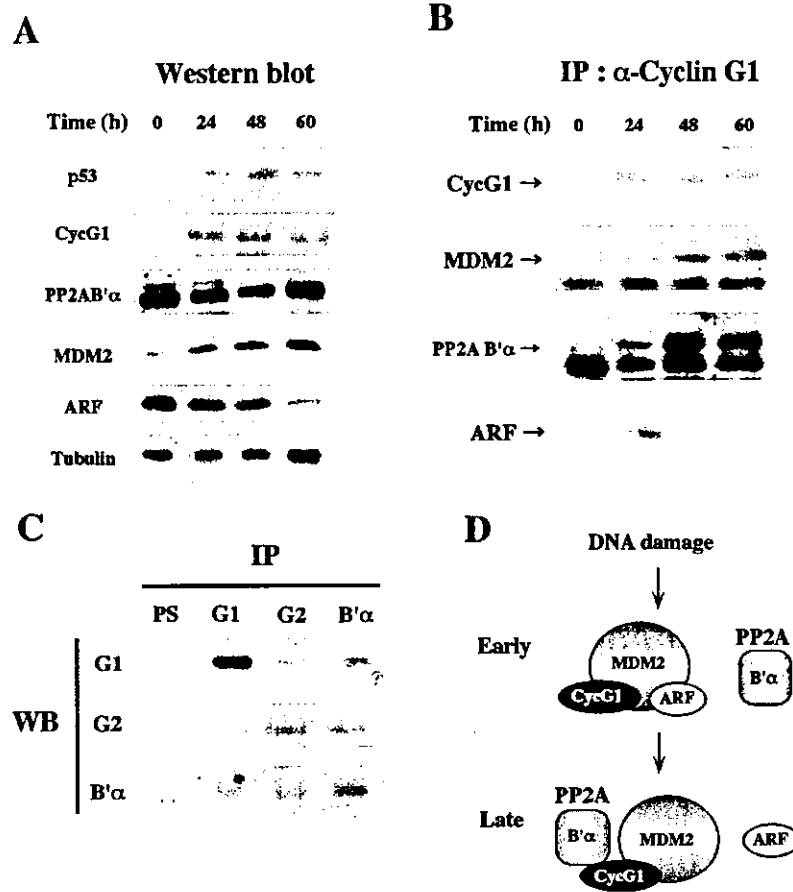| WB		PS	G1	G2	B'α
	G1				
	G2				
	B'α				

D

Figure 6 Differential composition of cyclin G1 immuno-complexes during the early and late periods of recovery from DNA damage. (A) Wild-type MEFs were irradiated with 10 Gy of γ-radiation and harvested at the indicated times. SDS-PAGE and Western blot analysis were carried out on lysates with anti-p53, anti-cyclin G1, anti-ARF, anti-PP2A B'α anti-MDM2 and anti-tubulin antibodies. (B) The lysates treated as in (A) were precipitated with anti-cyclin G1 antibody. Precipitates were subjected to Western blot analysis with anti-cyclin G1, anti-ARF, anti-PP2A B'α and anti-MDM2 antibodies. (C) Association of cyclin G1 and cyclin G2 with the PP2A B'α1. 293T cells were infected with the retroviral constructs, pBabePuro-cyclin G1 and pBabePuro-cyclin G2, then harvested for immunoprecipitation with the relevant antibodies at 48 h after infection. Subsequently, precipitates and lysates were subjected to Western blot analysis with anti-cyclin G1 (upper panel), anti-cyclin G2 (middle panel) and anti-PP2A B'α (lower panel) antibodies. (D) Time dependent exchange of the association partners of cyclin G1 after irradiation. ARF associates with cyclin G1 in the early period of recovery from DNA damage but is exchanged for ARF in the late period of recovery from DNA damage. MDM2 associates with cyclin G1 irrespective of the time after irradiation.

revealed that cyclin G1 could correct for the reduced expression of p53 following γ-irradiation in cyclin G1$^{-/-}$ MEFs (Fig. 5B). In cyclin G1$^{-/-}$ MEFs expressing cyclin G1, p53 protein accumulated within the first 24 h and then decreased within the next 72 h to reach a level similar to that found in wild-type cells. The level of p53 at 72 h in cyclin G1$^{-/-}$ MEF expressing cyclin G1 was markedly decreased compared to that of cyclin G1$^{-/-}$ MEFs (Fig. 5B). These results show that cyclin G1 down-regulates p53 expression during the 48-h period following irradiation, suggesting that cyclin G1 can promote both p53 accumulation and degradation during the early and late periods following irradiation, respectively.

Altered composition of cyclin G1 immuno-complexes during the early and late periods following irradiation

As described above, we identified MDM2 as a novel association partner of cyclin G1 and cyclin G2. Consid-

ering that the B'α subunit of PP2A is shown to associate with cyclin G1 (Okamoto et al. 1996), we wondered if the expression profiles of these factors change in wild-type MEFs before and after DNA damage. Western blot analysis revealed that the level of B'α subunit of PP2A remained constant following DNA damage, but that the levels of MDM2 and ARF increased and decreased, respectively, following DNA damage (Fig. 6A). Using lysates from the irradiated cells, we further carried out immunoprecipitation with anti-cyclin G1 antibody (Fig. 6B). At 24 h after irradiation, MDM2 and ARF were co-precipitated with cyclin G1 but the amount of these co-immunoprecipiates containing PP2A were decreased (Fig. 6B, lane 2). We also performed a similar experiment using cyclin G1$^{-/-}$ cells that express retrovirally introduced cyclin G1 (data not shown). In this experiment, MDM2 and ARF were found to be co-precipitated with cyclin G1, but no co-immunoprecipitates containing PP2A could be detected (data not shown). These results are consistent with the results shown above

(Figs 3 and 4). At 60 h, however, cyclin G1 was no longer associated with ARF, although it is still associated with PP2A (Fig. 6B, lane 4). When cyclin G1$^{-/-}$ MEFs, exogeneously expressing cyclin G1 and cyclin G2, were irradiated, we found that cyclin G1 and cyclin G2 co-immunoprecipitated with PP2A (Fig. 6C). In Fig. 2C, we were also able to demonstrate that cyclin G2 co-immunoprecipitates with the MDM2-ARF complex. These results indicate that cyclin G2 associates not only with PP2A but also with the MDM2-ARF complex in vivo.

A schematic diagram (Fig. 6D) shows the changes that occur in the association partners of cyclin G1 in response to DNA damage. Following DNA damage, cyclin G1 is induced and associates with MDM2-ARF to prevent p53 ubiquitination by MDM2 during the early period following DNA damage. This allows p53 to play roles in cell cycle arrest and DNA repair. When DNA damage is repaired, the cyclin G1/MDM2 complex associates with PP2A to promote p53 degradation.

Discussion

ATM plays a role in the stabilization of p53 in response to double-strand DNA breaks, whereas ATR stabilizes p53 in response to UV-induced DNA damage. We reported previously that cyclin G1$^{-/-}$ MEFs have reduced cell survival after both ionizing and UV radiation (Kimura et al. 2001). In the present study, we have shown that p53 accumulation was decreased in cyclin G1$^{-/-}$ MEFs not only after γ irradiation but also after UV irradiation (Fig. 1A and B). These results suggest that the stabilization of p53 by cyclin G1 is independent of both the ATM and ATR pathways. In response to DNA damage, AT and Chk kinases phosphorylate p53 and inhibit the association of MDM2 with p53. In this process, ARF may help to localize MDM2 to the nucleolus, thereby separating MDM2 from p53 (Fig. 4A). Our demonstration of the dependence of association between MDM2 and ARF on cyclin G1 in vivo suggests that cyclin G1 is involved in the regulation of ARF-MDM2 complex formation as part of the process of p53 stabilization. Our results also suggest that cyclin G2 may also mediate the same process.

The process of p53 activation involves two steps. The first step involves the induction of p53 protein (Fig. 1A and B, time for 0−6 h), and the second step involves the accumulation of p53 (Fig. 1A and B, 6 h after). Although decreased accumulation of p53 in cyclin G1$^{-/-}$ cells was observed (Fig. 1A and B), the level of induction of p53 was similar in both wild-type and cyclin G1$^{-/-}$ cells after γ-irradiation (Fig. 1A and B, time for 0−6 h). A possible

explanation for this is that phosphorylation of p53 in response to DNA damage by AT and Chk kinases contributes to the first step of p53 induction. Cyclin G1, and also cyclin G2, could then promote the second step of p53 accumulation by regulating the association of MDM2 with ARF (Fig. 5B). Our results indicate that cyclin G1 regulates the accumulation of p53 protein, and directly associates with MDM2 to regulate the interaction of MDM2 with ARF. These results strongly suggest that cyclin G1 regulates p53 via MDM2 regulation. Both cyclin G1 and MDM2 genes are transcriptional targets of p53 (Donehower et al. 1992; Barak et al. 1993) whose expression is induced in response to DNA damage. Taken together, it seems reasonable to suggest that the transcriptional targets of p53 play roles as both positive and negative regulators of p53 accumulation.

Several groups have reported that ARF associates with MDM2 and sequesters it into the nucleolus to induce p53 protein in the nucleoplasm (Zhang et al. 1998; Honda & Yasuda 1999; Weber et al. 1999). We also report here that the accumulation of p53 protein in response to DNA damage was remarkably reduced by disruption of the cyclin G1 gene (Fig. 1), and that cyclin G1 directly associates with MDM2 in vitro (Fig. 3). These results suggest that cyclin G1 regulates the level of p53 protein via MDM2 regulation. Weber et al. reported a direct interaction between MDM and ARF in vitro in the absence of cyclin G1 expression (Weber et al. 2000). We also found that the in vitro association of MDM2 and ARF was independent of cyclin G1 (Fig. 3). These results indicate that ARF is able to associate with MDM2 without cyclin G1 in vitro. However, without cyclin G1 over-expression in cyclin G1$^{-/-}$ MEFs (Fig. 1) and 293T cells (Fig. 4), we could not detect the association of ARF with MDM2. This result indicates that cyclin G1 expression is required for the association of ARF with MDM2 in vivo.

Figure 5 indicates that disruption of the cyclin G1 gene causes a deficiency not only in p53 induction and accumulation during the early periods of recovery from DNA damage but also in p53 degradation during later periods. These results lead to the following conclusion. DNA damage causes the activation of AT and Chk kinases which then phospholylate p53 at serine 15 and 20. These phosphorylations disturb p53 ubiquitination by MDM2, activate the p53 protein, and induce the transcriptional targets of p53, including MDM2 and cyclin G1. Then, cyclin G1 sequesters MDM2 to the nucleolus via the ARF pathway until the DNA damage is repaired. At later periods, the cyclin G1-MDM2 complex associates with PP2A, which promotes p53 degradation. Dephosphorylation of MDM2 by PP2A may promote the ubiquitination of p53 by MDM2 and